CARBON NANOTUBES TOWARDS SOLAR CELL APPLICATION

Ph.D Thesis

March 2012

Approved by

Professor Tetsuo Soga
Dissertation Academic supervisor

Ishwor Khatri

Department of Frontier Materials
Graduate School of Engineering,
Nagoya Institute of Technology, Japan

CONTENTS **TITLE** **PAGE**

CHAPTER 1

CARBON MATERIALS FOR SOLAR CELLS

Introduction

Carbon was discovered in prehistory and has been known since ancient time. But it was recognized as an element only in the 18th century. It is one of the versatile element and the most abundant element in the universe. It is a material of highly stable, cheap and non-toxic, which can be obtained from precursors sufficiently available in nature.

Carbon is a remarkable element existing in a variety of stable forms ranging from insulator/semiconducting diamond to metallic/semi metallic graphite to conducting/semi conducting nano/micro tubes to fullerenes of highest order of symmetry, which show many interesting optoelectronic properties. It has the ability to bond with itself and a wide variety of other elements. In addition, it is a very special element as it plays a dominant role in the chemistry of life. There are four known allotropes of carbon. They are graphite, diamond, fullerene and carbon nanotubes (CNTs).

1.1 Allotropes of carbon

1.1.1 Graphite

Graphite is one of the allotropes of carbon. It can conduct electricity because of the large number of electron delocalization within the carbon layers. These electrons are free to move, so are able to conduct electricity. The crystal structure of graphite consists of layers in which the carbon atoms are arranged in an open honeycomb network as shown in Fig 1.

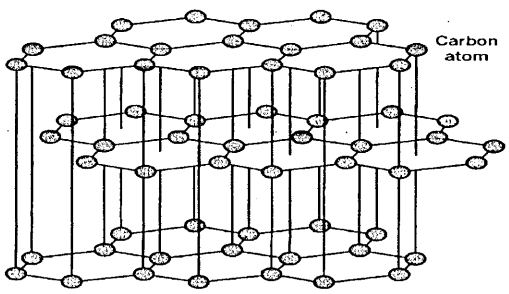

Figure 1. The crystal structure of graphite.

Each carbon atom is covalently bonded to three other surrounding carbon atoms. The flat sheets of carbon atoms are bonded into hexagonal structures. They exit in layers, which are not covalently connected to the neighboring layers. The unit cell dimensions are a=b=2.456A. The C-C bond length in the bulk form is 1.418 A, and the interlayer spacing is c/2=3.347A [1].

1.1.2 Diamond

Diamond is another crystalline form of carbon, generally know as a gemstone. It is transparent crystal of pure carbon consisting of tetrahedral bonded carbon atoms. The ideal diamond structure has two distinct carbon sites and has the characteristic property that every carbon atom is surrounded by four other carbon atoms and made a strong covalent sp^3 bond. The length of nearest carbon-carbon (C-C) is 1.54A nearly 10% larger than in graphite. The crystal structure of diamond is shown in Fig. 2

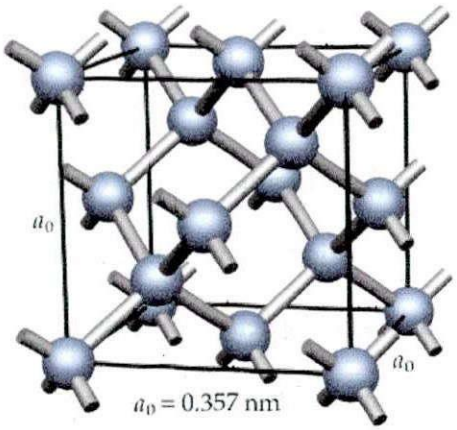

Figure 2. The crystal structure of diamond

Diamond has many outstanding properties such as extremely hardness (~90Gpa), high density (3.52 g/cm^2), good electrical insulator (room temperature resistively ~10^{16} Ω.cm.). It is used for cutting, drilling, lapping, grinding, polishing etc.

1.1.3 Fullerenes

Eiji Osawa of Toyohashi University of Technology predicted the existence of C_{60} (fullerenes) in the year of 1970. He made some hypothesis about ball shape carbon structure. He published that report in Japanese magazine and did not reach to the people of other country [2]. Real breakthrough came when Robert Curl, Harold Kroto and Richard Smalley first reported the existence of fullerene in the year of 1985 [3]. They consist of a spherical, ellipsoid or cylindrical arrangement of many carbon atoms, which were later named as "fullerences" are sometimes called "buckyballs". The smallest buckyball consists of 20 carbon atoms and largest one has about 540 carbon atoms. The most common size has 60 or 70 carbon atoms. The structure of C_{60} is shown in Fig. 3, which resembles a round soccer ball of the type made of hexagons and pentagons with carbon atom at the corners of each hexagons and a bond along each edge.

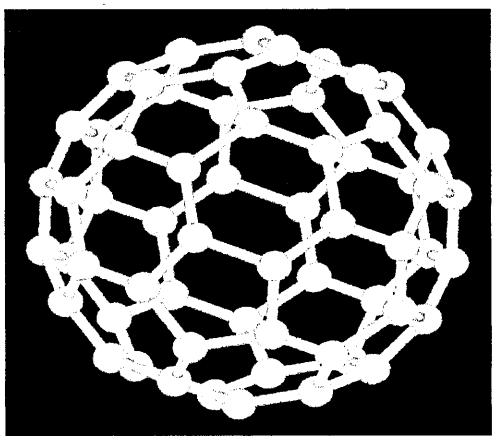

Figure 3. The crystal structure of fullerenes

1.1.4 Carbon nanotubes

Bulk graphite can be thought of as the parent material of graphene (2 dimentional). Fullerences is considered as zero dimentional carbon material. So, one can imagine the existence of one dimentional carbon material. Scientists need to wait until 1991 to

examine the experimental existence of 1D rolled up graphene sheet. Sumio Ijima's work highlighted the noble properties of needle like wrapped graphene sheets (so called carbon nanotubes) [4]. The prefix 'nano' is used because the diameter is on the nanometer scale (1 nm = 10^{-9} m). It can be ranked as one of the most exciting scientific discovery. The name of the CNTs is derived from their size, since their aspect ratio is very high. It is a quasi-1D nanomaterial that exhibit extraordinary electronic properties such as high current carrying capability and reduced scattering rates.

CNTs is mainly classified into two basic forms, SWCNTs and MWCNTs. SWCNTs consist of a single tube of graphene (Fig. 4 (a)), whereas MWCNTs are composed of several concentric tubes of graphene fitted one inside the other [Fig 4(b)]. The diameter of CNTs varies from a few nanometres in the case of SWCNTs to several tens of nanometres in the case of MWCNTs. There is also a special class of MWCNTs called double-walled nanotubes (DWCNTs), which have different properties to SWCNTs and MWCNTs [Fig 4 (c)]. Despite such a small diameter, the length of SWCNT is many orders of magnitude

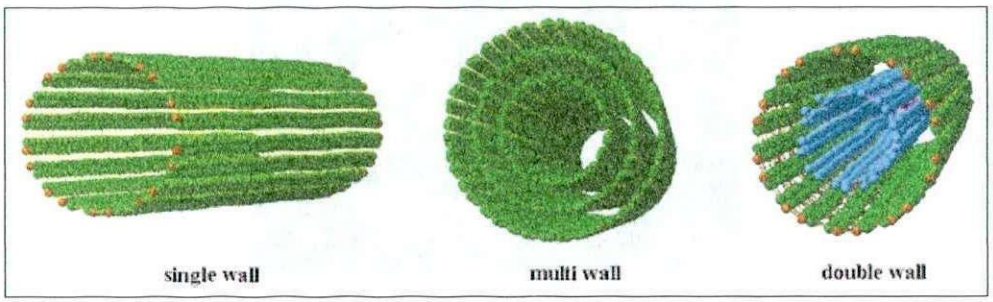

Figure 4. Different type of carbon nanotubes [Source 5].

Sidewall and end cap of CNTs possess different physical and chemical properties. It is believed that end cap is more reactive than the sidewall. The end cap structure is similar to smaller fullerene structure such as C_{60}. CNTs have begun to be widely used in

many applications due to their unique electrical, mechanical, optical and thermal properties. The application of CNTs is usually given by the CNTs structure (number of walls, diameter, length, chiral angle, etc.), which gives them the specific properties. The possible applications of CNTs include conductive films, solar cells, fuel cells, supercapacitors, transistors, memories, displays, separation membranes, filters, purification systems, sensors, clothes, etc.

1.2 Synthesis of carbon nanotubes

There are different methods for the synthesis of carbon nanotubes. Some of the main methods are summarized here.

1.2.1 Arc discharge

In 1991, Sumio Iijima first prepared CNTs [4] by arc discharge method and the macroscopic production of CNTs was made in 1992 [6]. This method is very well known to prepare SWCNTs, DWCNTs and MWCNTs. In arc discharge method, direct current (DC) arc discharge experiments were carried out in a stainless steel chamber that was filled with hydrogen/helium, or their mixture at certain pressure. The anode is a graphite rod in which a hole had been drilled and filled with some metal catalyst. The anode and cathode was kept at certain distance. When current was passed through the electrodes, plasma will be generated. This plasma will evaporate the carbon on the anode and the material will be deposited on the cathode surface. Using this method Iijima et al. [7] and Bethune et al. [8] synthesized SWCNTs. DWCNTs is also synthesized by this method [9,10].

1.2.2. Laser ablation technique

In this method, the optimum background gas and catalyst mixture is same as in the arc discharge method. In the year of 1995, Smalley's group prepared CNTs by laser ablation method. There are two kinds of laser to vaporize the graphtic target. These are continuous laser and pulsed laser. The light intensity of pulsed laser is much higher than the continuous laser. The chamber is filled with inert gas (helium or argon) in order to keep the pressure at 500 Torr. Continuous or pulsed laser was used to vaporize a target consisting of a mixture of graphite and metal catalyst (cobalt or nickel). As the vaporized species cooled down, small carbon molecule quickly condense to form large clusters. The catalyst also started to condense and adheres to carbon clusters to prevent their closing into cage structures. The SWCNTs formed in this case are bundle together by Van der Walls force. In the case of pure graphite electrodes, MWCNTs would form but SWCNTs can be synthesized using mixture of graphite with transition metals as a catalyst.

1.2.3 Chemical vapor deposition (CVD)

CVD method is cost effective and viable techniques for large-scale production of CNTs. Recently this method has created a lot of attention because of high yield, low impurity and bulk production of CNTs at moderate temperature. This method is capable to control diameter, length and alignment of the CNTs by choosing suitable parameters. It mainly involves the decomposition of hydrocarbon (ethylene, acetylene, methane etc) over the transition metal catalyst at desired temperature. CVD method is essentially a two-step process consisting of a catalyst preparation followed by the synthesis of CNTs. Different kinds of CVD techniques are developed to synthesize CNTs (SWCNTs, DWCNTs, MWCNTs). Some are plasma enhanced CVD [12-14], thermal CVD [15], alcohol catalytic CVD [16,17], aero gel supported CVD [18]. In some applications, the

deposition of CNTs on substrate is highly desirable. In this regard CVD method is superior compared to laser ablation and arc discharge method. The CNTs deposited on the substrate are highly aligned due to Van der Walls interaction between the neighboring CNTs. Various groups reported the highly aligned CNTs on different substrates by this simple method [19-23].

1.2.4 Spray pyrolysis method

It is very simple, effective and inexpensive method for the synthesis of CNTs. With this method, Afre et al. synthesized well-aligned MWCNTs from natural precursor [24]. Spray pyrolysis method is promising method for the growth of different kind of CNTs.

1.2.5 Ultrasonic spray pyrolysis

Ultrasonic spray pyrolysis is new and simple method to synthesis carbon nanomaterials (SWCNTs, MWCNTs, CNFs, CNWs). It mainly consists of three sections viz atomization unit, a transportation system and an electrical furnance with a large quartz tube [25]. It is very simple method for the synthesis of carbon nanomaterials. During my study, I synthesized CNTs by ultrasonic spray pyrolysis and use it with semiconducting organic material for the fabrication of hybrid solar cell.

1.3 Solar Energy and its application

Solar energy is the source of life on the earth via photosynthesis; man eats vegetables and trees grown using solar light. Human have manipulated solar energy since the 7th century B.C, when magnifying glasses were used to concentrate the sun's rays to make fire and to burn papers. Development of solar cells started from the pioneering work of French physicist Alexander Becquerel in 1839[26], who discovered the photovoltaic effect. In 1873, Willoughby Smith discovered the photoconductivity of selenium. In 1876, William Adams and his student Richard Day [27] discovered that

selenium produces electricity when exposed to light. However, those selenium solar cells failed to convert enough sunlight into electricity. In 1883, Charles Fritts developed the first solar cells by coating a semiconductor, selenium, with a nearly transparent layer of gold. These cells were very inefficient, that produces less electrical energy.

The better understanding of the physical principle involving solar cell's photoelectric effect is provided by Albert Einstein 1905 in his paper. In 1914, Robert Millikan provided experimental proof of the photoelectric effect. The effect was then put on hold until the discovery of transistors and the explanation of the physics of the p-n junction by Shockley [28], Bardeen and Brattain [29] in 1949. Then, in 1954, photovoltaic technology was born in the US when Daryl Chapin, Calvin Fuller and Gerald Pearson [30] developed the silicon photovoltaic cell at Bell Laboratory. The first solar cell was based on crystalline silicon (c-Si) and had an efficiency of 6%. Since then, a variety of commercial and government entities have worked to develop practical applications of photovoltaic cells and efficiency was increased up to around 10 % in a couple of years.

Today PV solar energy is one of the most promising and reliable sources of alternative energy. The direct conversion of solar radiation into electricity through the process of photovoltaics has a number of advantages to solve power demand. The term photovoltaic comes from the Greek "phos" which means light and "volt", from the scientist Alessandro Volta. In other words, photovoltaic literally means "light-electricity". PV cell is a device that produces usable electrical energy when light falls on it. PV conversion systems tap an inexhaustible resource, which is free of charge and available anywhere in the world. The energy supply form the sun is truly enormous; on average, the Earth's surface receives about 1.2×10^{17} W of solar power. This means that in less than one hour, enough energy is supplied to the Earth, which is sufficient for energy demand of the human population over the whole year [31].

1.4 World power demand and energy sources

Fig. 5 shows global energy consumption over the next several decades. It is likely that only the use of traditional fossil fuels will decline, whereas use of other energy souces (like solar, wind, geothermal, nuclear power) will grow providing an increasing energy demand of modern society.

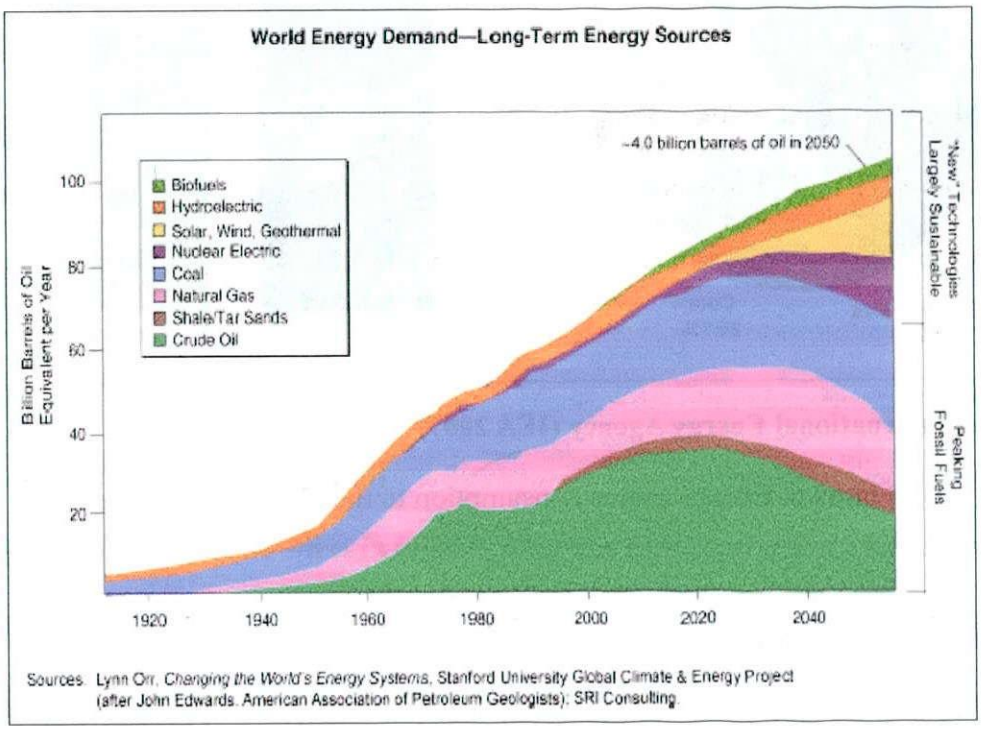

Figure 5. World energy demand.

Figure 6 shows the principle energy sources currently being used by mankind, which shows the heavy dependence on fossil fuel. In order to meet the power demand scientist researches on safe, reasonable and environment friendly energy sources. Renewable energy technologies (e.g solar, wind and others) have emerged as alternatives to worldwide energy problems, as they are nonpolluting, inexhaustible. Unlike traditional fossil fuels, which contribute to a lot of environmental problems, such as air pollution, water and soil contamination whereas renewable energy contributes very little or no such problems. Among the renewable energy technologies, PV solar

energy conversion is the most popular and reliable source of renewable energy for the future. According to International Energy Association (IEA, 2007), solar energy covers 0.039% of the world energy demand.

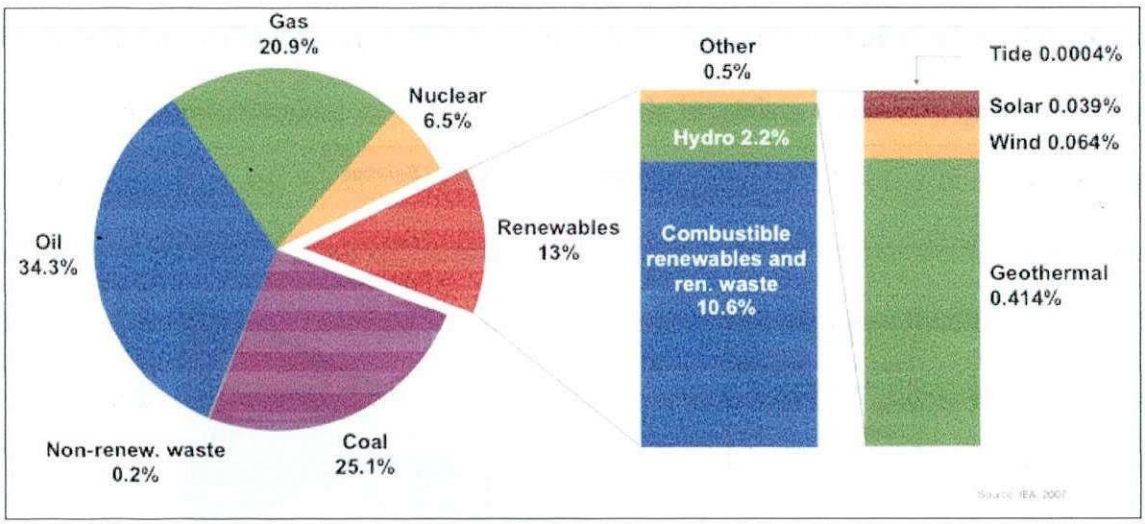

Source: International Energy Agency (IEA 2007)

Figure 6. Energy source consumption to the global energy need.

1.5 Materials for solar cell

Solar cells are made from various semiconductor materials. A semiconductor is a material that becomes electrically conductive when supplied with light or heat, but it behaves as an insulator at low temperatures. A solar cell converts sunlight into electricity, either directly through the PV effect, or indirectly by first converting the solar energy to heat or chemical energy. In semiconducting material electrons live in range of define energy level called band. The conduction band is partially filled with electrons, creating negative charge. The valance band has areas where electrons are missing-known as hole (positive charge). In the absence of light, the positive and negative charges balance each other in the case of intrinsic semiconductors. When light energy strikes on semiconductor pn junction, the electrons are dislodged causing

electrons to move down an external circuit in the form of light-generating electricity. This phenomenon is called PV effect. Detail theoretical description is given in ref [32]. If light with photon energy is greater than optical band gap, free electrons and free holes are formed by optical excitation in the semiconductor. Different materials used for solar cells are: silicon (Si), copper indium gallium selenide [$Cu(In,Ga)Se_2$], cadmium sulfide (CdS), cadmium telluride (CdTe), titanium dioxide (TiO_2) etc. silicon and compound semiconductor-based devices are dominating solar technology. However, the cost of these solar cells is high. So, low cost and high efficiency solar cells are yet to be realized for the commercialization. Organic solar cell is one of the promising low cost solar materials for future energy.

1.6 Basic of organic solar cell

Since the photovoltaic effect in organic solid was first observed in 1959 in anthracene crystals [33], three main solid-state device concepts have been emerged.

1.6.1 Organic solar cells based on vacuum deposited small molecules

The device concept is based on the thermal evaporation of at least two n- and p-conducting materials. Excitons are generated due to the absorption of light in the respective organic materials. These excitions have to travel to an interface between the n- and p-conducting layers. Due to the energetical conditions, they splitted into free electrons and holes. Finally the respective charge carriers are transported towards their electrodes. As shown in Fig. 7 (a) and Fig. 7(b), p-n junctions can be realized as heterojuncitons or as well as interpeneatrating networks (bulk heterojunctions) respectively.

For the fabrication of the first small molecule organic solar cells, chlorophyll like low molecular weight dyes based on on phthalocyanines and porphyrins were used [34].

Since Tang [35] presented a 1% efficient bilayer heterojuntion solar cell based on copper phthalocyanine (CuPc) and a perylene tetracarboxylic derivative (PTCBI) in 1986, enormous progress was made in research.

The fabrication under high vacuum is the main advantage of this type of solar cell. The well-defined fabrication environment ensures a very high reproducibility of the devices. Unfortunately, high vacuum technology is very expensive and complex to handle.

1.6.2 Polymer based organic solar cells

The device architectures of polymer solar cells are similar to those used for small molecule cells. However the fabrication differs significantly. Since polymers have a very high molecular weight, they can`t be thermally evaporated. Heterojunction and bulk heterojunction polymer cells are therefore solution processed. Semiconducting polymers such as P3HT (poly (3-hexylthiophene)) in combination with the fullerence (C_{60}) gain higher power conversion efficiencies. Deposition of organics by screen-printing, doctor blading, inkjet printing, and spray deposition is possible because these materials can be made soluble. Additionally, these deposition techniques are done at low temperature, which allows devices to be fabricated on plastic substrates for flexible devices. No expensive vacuum technology is needed which is another advantage of this solar cell towards commercialization.

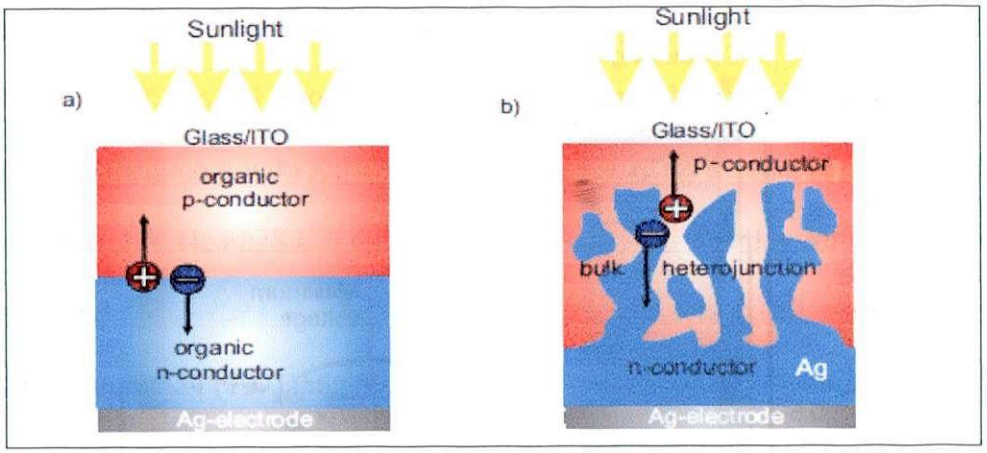

Figure 7. Device setup of a heterojunction solar cell. (a) p-conducting material forms a heterojunction with an n-conducting material in such a way, that excition dissociation into free charge carriers is energetically favorable (b) Device setup of a bulk heterojuntion solar cell. Here the simple heterojuntion is enhanced at the interface area by an interpenetrating network of n- and p-conducting materials.

1.6.3 Dye-sensitized solar cell

Another cell concept is the dye sensitized solar cell shown in Fig 8. This concept has attracted wide attention since its invention in 1991 by M. Gratzel [36]. It is based on a mesoporous nanocrystalline TiO_2 film that is attached to a transparent FTO electrode. The particles in the TiO_2 film are covered by a monolayer of dye. The counter electrode is contacted through a liquid electrode or an organic p-conductor, which penetrates into the pores of the TiO_2 network. When a dye molecule is excited by light, it injects electron into the TiO_2, creating a positively charged dye molecule. This phenomenon produces the charge separation required for photovoltaic cells. The electrons are donated from the counter electrode via the electrolyte to the positively charged dye on the TiO_2 surface, returning the dye molecules to their original state.

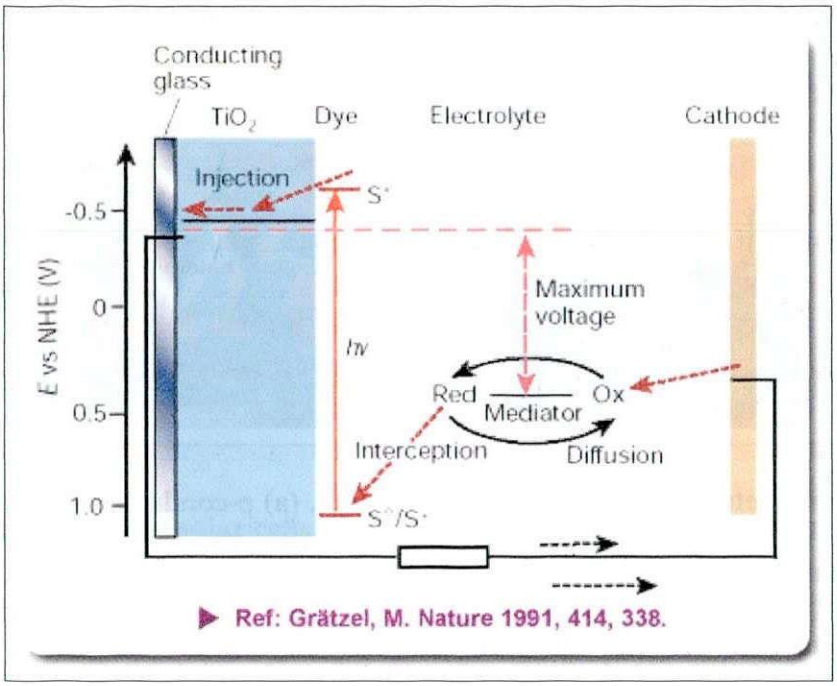

Figure 6. Schematic structure material of a dye-sensitized solar cell. In this cell concept, a mesoporous nanocrystalline TiO_2 film is attached to a transparent electrode. The particles in the TiO_2 film are covered by a monolayer of dye. The counter electrode is contacted through a liquid electrolyte or a p-conductor, which penetrates the pores of the TiO_2 network.

On the other hand, organic p-type semiconducting hole transport materials are gaining substantial interest to fabricate solid-state dye sensitized solar cell. After spin coating semiconduting material on the surface of the dye sensitized TiO_2 layer, metal electrodes are thermally deposited to complete the solar cell fabrication process. This thermally deposited metal electrode may create large parasitic resistance and damage the polymeric layer. Thus the device performance may reduce. To overcome these problems, we introduce lamination process for the fabrication of solid-state dye sensitized solar cell, which is described in chapter 4.

References:

[1] R.W.G. Wyckoff, Crystal Structure, Vol.1, (Interscience, New York, 1964)

[2] http://en.wikipedia.org/wiki/Fullerene

[3] H. W. Kroto, J.R. Heath, S.C. Obrien, R.F. Curl and R.E. Smalley *Nature* **318** (1985) 162 - 163

[4] S.Iijima, Nature 354 (1991)56.

[5] R. Niessen, Electrochemical hydrogen storage in lightweight electrode materials, Ph.D. thesis, Technische Universiteit Eindhoven (2006)

[6] T.W. Ebbesen and P.M. Ajayan, Nature 358 (1992) 220.

[7] S. Iijima and T. Ichihashi, Nature 363 (1993) 603.

[8] D.S. Bethune, C.H. Klang, M. S. DeVries, G. Gorman, R. Savoy, J. Vazquez, R. Beyers, Nature 363 (1993) 605.

[9] J. L. Hutchison, N.A. Kiselev, E. P. Krinichnaya, A. V. Krestinin, R.O. Loutfy, A. P. Morawsky, V. E. Muradyan, E.D. Obraztsova, J. Sloan, S.V. Terekhov, D.N. Zakharov, Carbon 39 (2001) 761.

[10] Y. Saito, T. Kakahira, S. Uemura, J. Phys. Chem. B 107 (2003) 931.

[11] T. Guo, P. Nikolaev, A. G. Rinzler, D. Tomanek, D.T. Colbert, R.E. Smalley, J. Phys.Chem. 99 (1995) 10694.

[12] Y. Li, D. Mann, M. Rolandi, W. Kim, A. Ural, S. Hung, A. Javey, J. Cao, D. Wang, E. Yenilmez, Q. Wang, J. F. Gibbons, Y. Nishi, H. Dai, Nano Lett. 4 (2004) 317.

[13] Yo-Sep Min, E. J. Bae, B. S. Oh, D. Kang, W. Park, J. Am. Chem. Soc. 127 (2005) 12498.

[14] N. A. Kiselev, J. L. Hutchison, A. P. Moravsky, E. V. Rakova, E.V. Dreval, C.J.D. Hetherington, D.N. Zakharov, J. Sloan, R.O. Loutfy, Carbon 42 (2004) 149.

[15] H. Liao and J.H. Hafner, J. Phys. Chem. B 108 (2004) 6941.

[16] Y. Murakami, Y. Miyauchi, S. Chiashi, S. Maruyama, Chem. Phys. Lett. 377 (2003) 49.

[17] S. Maruyama, R. Kojima, Y. Miyauchi, S. Chiashi, M. Kohno, Chem. Phys. Lett. 360 (2002) 229.

[18] M. Su, B. Zheng, J. Liu, Chem. Phys. Lett. 322 (2000) 321.

[19] J. Liu, X. Li, A. Schrand, T. Ohashi, L. Dai. Chem. Mater. 17 (2005) 6599.

[20] Y. H. Li, C. Xu, B. Wei, X. Zhang, M. Zheng, D. Wu, P.M. Ajayan, Chem. Mater. 14 (2002) 483.

[21] Y. Yang, S. Huang, H. He, A.W.H. Mau, L. Dai, J. Am. Chem. Soc. 121 (1999) 10832.

[22] S. Fan, M. Chapline, N. Franklin, T. Tombler, A. Cassell, H. Dai, Science 283 (1999) 512

[23] M. Terrones, N. Grobert, J. Olivares, J.P. Zhang, H. Terrones, K. Kordatos, W.K. Hsu, J.P. Hare, P.D. Townsend, K. Prassides, A.K. Cheetham, H.W. Kroto, D.R.M. Walton, Nature 388 (1997)52.

[24] R.A Afre, T. Soga, T. Jimbo, M. Kumar, Y. Ando, M. Sharon, Chem. Phys. Lett. 414 (2005) 6.

[25]. I. Khatri, T.Soga, T. Jimbo. S. Adhikari, H.R.Aryal. M.Umeno. Diamond and Related Material 18 (2009) 319.

[26] A.E. Becquerel, Compt. Rendus de L" Academie des Sciences, 9 (1839) 561.

[27] W. Adams, R. Day, Proc. Roy. Soc. A 25 (1877)113.

[28] W. Shockley, Bell Syst. Tech. Journ. 28 (1949) 435.

[29] J. Bardeen and W.H. Brattain, Phys. Rev. 74 (1948) 230.

[30] D. M. Chapin, C.S. Fuller, G.L. Pearson, J. Appl. Phys. 25 (1954) 676.

[31] T. Markvart, Solar Electricity, 2nd Edition, University of Southampton, UK, Chapter 1, pp. 131.

[32] T. Soga: Nanostructured Materials for Solar Energy Conversion, Chapter 1. Elsevier, Amsterdam (2006)

[33] H. Kallmann and M. Pope. J. Chem. Phys 30 (1959) 585.

[34] C.W Tang and A.C. Albrecht. J. Chem. Phys 62 (1975) 2139.

[35] C.W. Tang and S.A. VanSlyke. Appl. Phys. Lett. 51 (1987) 913.

[36] B. O'Regan and M. Gr¨atzel. Nature 353, (1991) 6346.

1.7 Purpose and organization of dissertation

The purpose of this study is to improve photovoltaic properties of solar cells by incorporating CNTs. Here, I describe the synthesis of CNTs by ultrasonic spray pyrolysis method and use it with organic materials to fabricate hybrid solar cell. CNTs are synthesized on silicon and zeolite supporting material. As-grown CNTs are purified by different techniques. Purified CNTs are functionalized by acid treatment to fabricate solar cell. The overall story has been summarized into following chapters.

In chapter 1, a short description on different forms of carbon is given. The different synthesis processes of CNTs are included. It also includes a short note on organic and dye sensitized solar cells.

In chapter 2, a brief description on the synthesis of CNTs by ultrasonic spray pyrolysis is given. In optimized parameter, SWCNTs are synthesized on silicon and zeolite supporting material. The growth mechanism of CNTs on zeolite particles is analyzed. In another experiment, SWCNTs are deposited on desire substrate at low temperature by placing substrate at downstream of the tube.

In all of these experiments, alcohol and nitrogen are used as carbon and carrier gas respectively. As-synthesized materials are characterized by SEM, TEM, UV-vis-NIR and Raman spectroscopy.

In chapter 3, application of carbon nanotubes towards organic solar cell is given. The semiconducting polymer poly (3-octylthiophene) [(P3OT)] was mixed with SWCNTs and functionalized MWCNTs (f-MWCNTs) to fabricate heterojunction solar cell. The performance of the device was improved by manyfold by the incorporation of both SWCNTs and f-MWCNTs. The open circuit voltage (V_{oc}), short circuit current density (J_{sc}), fill factor (FF) and power conversion efficieny (η) were 0.44V, 6.16 mA/cm^2, 36%, and 0.98%, respectively. We expect that SWCNTs help in exciton

dissociation and provide percolating paths for electron transfer, whereas f-MWCNTs provide efficient hole transportation. CNTs incorporations yields better carrier mobility, easy exciton splitting, and suppression of charge recombination, therby improving photovoltaic action.

Chapter 4 examines the characterization of laminated dye sensitized solar cell (s-DSSC). Solid-state DSSCs using organic materials as hole transport material by hot plate lamination process is fabricated. At present, efficiency (η) of the device is low, but it is a promising method for future energy source as they are cheaper, light weight, flexible and can be made into large areas by roll-to-roll processing, which are showing growing importance.

In Chapter 5, the overall summary of the thesis and the suggested future work is presented. I am very interested to fabricate multilayer hybrid solar cell from hot plate lamination technique.

CHAPTER 2

SYNTHESIS OF CARBON NANOTUBES BY ULTRASONIC SPRAY PYROLYSIS

CHAPTER 2
SYNTHESIS OF CARBON NANOTUBES BY ULTRASONIC SPRAY PYROLYSIS

2.1 Introduction

Carbon nanomaterials are available in different forms such as carbon nanotubes (CNTs), carbon nanofibers (CNFs), carbon nanowalls (CNWs), graphite, graphene etc. Interestingly, all these nanomaterials have unique physical, chemical, electrical and mechanical properties, which attract a lot of attentions of researchers. These carbonaceous nanomaterials are applicable to various electronic devices such as fuel cells, electron field emitters, solar cell etc. Suitable parameters during their synthesis processes can control the morphological structure and growth rate. There are several methods to synthesis carbon nanomaterials. Arc discharge [1, 2, 3], laser ablation [4, 5, 6], chemical vapor deposition [7, 8, 9], alcohol chemical vapor deposition [10, 11] are well-established methods. Expensive devices equipped with different gases and carbon sources are being used for the synthesis of these carbon nanomaterials, which may not be available everywhere. Hence, simple and inexpensive methods are still required. Recently we introduced ultrasonic spray pyrolysis method for the synthesis of various carbon nanomaterials including single wall carbon nanotubes [12], multi wall carbon nanotubes [13,14], carbon nanofibers [15,16], carbon nanowalls [17] and pure SWCNTs and CNWs at low substrate temperture [17,18].

Since the system is new and interesting, we tried to investigate it from every angle by placing substrates at different positions inside the quartz tube with and without using catalyst particles. The advantages of this single-step process are: (1) it doesn't require reducing agent and vacuum pump for the synthesis of SWCNTs [12, 18] (2) synthesis of both 1D [12-18] and 2D [17] carbon nanomaterials are possible (3) it is a simple and low cost system that is suitable for mass production [14] (4) More importantly, the system passes insoluble nanomaterials with the ethanol mist [15-17].

CHAPTER 2
SYNTHESIS OF CARBON NANOTUBES BY ULTRASONIC SPRAY PYROLYSIS

2.2 Ultrasonic spray pyrolysis

Figure 1(a) shows the schematic diagram of ultrasonic spray pyrolysis method. This method mainly consists of three sections called an atomization unit, a transportation system, and an electrical furnance with quartz tube.

Atomization unit has electric vibrators (Ultrasonic Humidifier with Oscillator Unit, 1.65 MHz, Atom Medical Corp., Model 303), which was applied indirectly via transmission medium liquid (water only) and 0.06 mm cup shaped plastic sheet (Medication Cup) where liquid precursor is kept. Medication cup separates transmission medium liquid (water) and liquid precursor (ethanol). Fig 1(b) shows the structure of atomic chamber (or internal structure of ultrasonic nebulizer).

Transportation system is a plastic pipes used to pass pure nitrogen gas (99.9%) and precursor mist inside quartz tube.

Electrical furnance is an electrical instrument, which generates high temperature for the synthesis of carbon nanomaterials. Quartz tube is put inside.

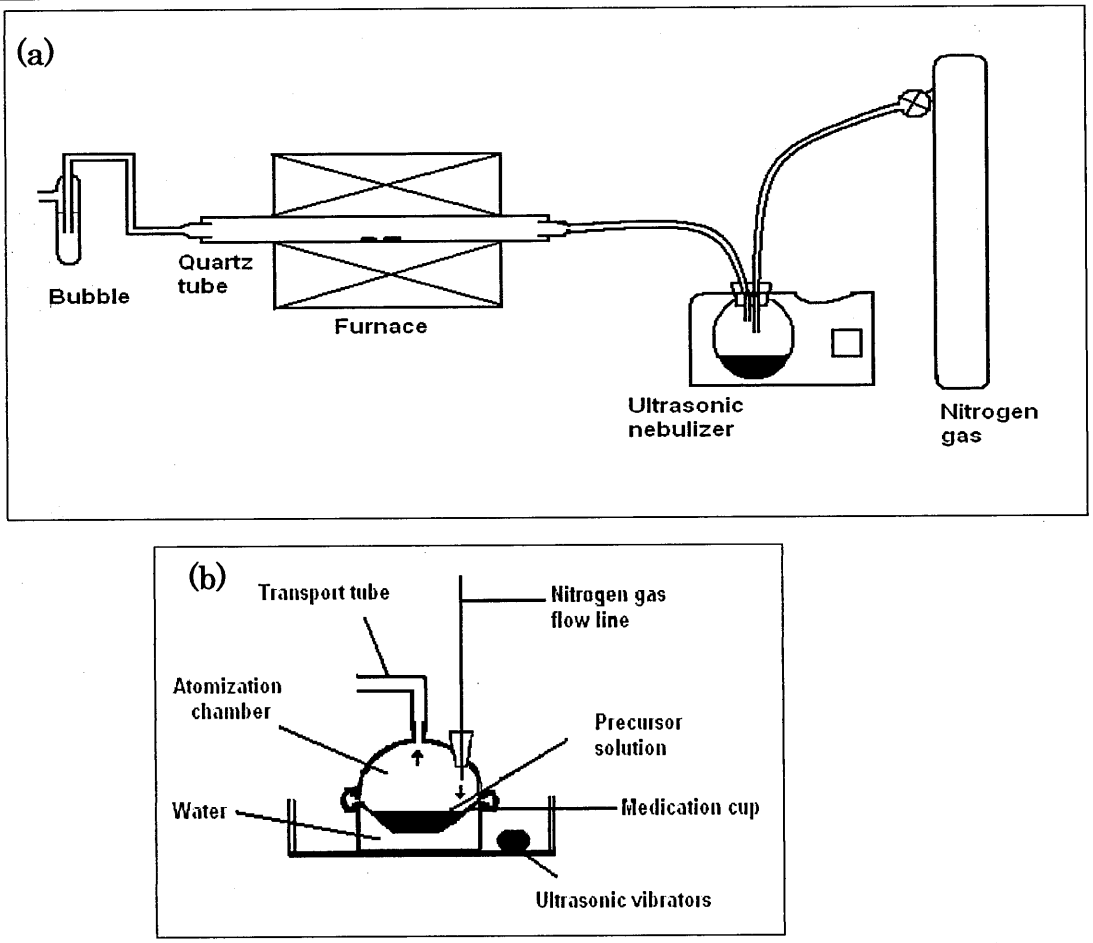

Figure 1. (a) Schematic diagram of ultrasonic spray pyrolysis set-up for synthesis of carbon nanomaterials. (b) Internal structure of ultrasonic nebulizer or atomization chamber

2.2.1 Characterizations

The morphology of as-grown materials was characterized by scanning electronic microscope (SEM), transmission electron microscopy (TEM) and Raman spectroscopy. SEM was performed on Hitachi S-3000H by placing as-grown samples on conductive carbon tape. For TEM studies, the samples were prepared by sonication of as-grown products in ethanol and a few drops of resultant suspension was put onto holey carbon grid and dried. TEM was performed by JEOL, JEM- 4000, EXII, electron microscope. Raman spectra of as-grown samples were performed by JASCO NRS-1500W, green

laser with excitation wavelength 532 nm. Ultraviolet/visible/near infrared (UV/vis/NIR) was performed by JASCO V-570.

2.3 Synthesis of SWCNTs on silicon substrates

2.3.1. Experimental details

The bimetallic catalysts molybdenum and cobalt was prepared as discussed in Ref [19]. $(C_2H_3O_2)_2Co$ (cobalt acetate 0.0438 wt.%) and $[(C_2H_3O_2)_2Mo]_2$ (molybdenum acetate dimer 0.02527 wt.%) were dissolved in ethanol and ultra-sonicated for 2 h. Cleaned substrates were dipped into it and the solution was evaporated at 80 °C. These substrates were put vertically, horizontally on a substrates holder in a quart boat and inserted into the middle of the large quartz tube. In each experiment, these substrates were heated to 400 °C for 5 min to change metallic acetate into metallic oxide. Then, both the ends of quartz tube were closed by quartz joints with nebulizer at one side and another side was connected to water bubbler. Nitrogen gas was kept in a constant flow of 2.0 l/min before reaching to the set temperature. When the reaction furnace reached to set temperature, N_2 gas flow increased to 2.5 l/min and waited for more 5 min. Mist of precursor flow was maintained by nebulizer. The morphology of as-grown materials was characterized by SEM, TEM and Raman spectroscopy.

2.3.2. Result and discussion

Figure 2 shows the typical Raman spectra of as-grown SWCNTs from dip coating. The G-band peak around 1590 cm^{-1} corresponds to tangential stretching mode (E_{2g}) of highly oriented pyrolytic graphite and suggests the materials are composed of crystalline graphitic carbon and the D-band peak near 1350 cm^{-1} originates from disorder in the sp^2 hybridized graphene sheets, tube ends etc. The radial breathing mode (RBM) between 180 cm^{-1} and 280 cm^{-1} are unique to SWCNTs [20]. G peak is comparatively higher than D peak. It suggests that that the system is suitable for

growing pure SWCNTs. Diameter of SWCNTs was calculated within 0.8 nm–1.2 nm. Raman spectra of SWCNTs were obtained throughout the polished surface of silicon substrates which indicate the reproducibility of the SWCNTs process.

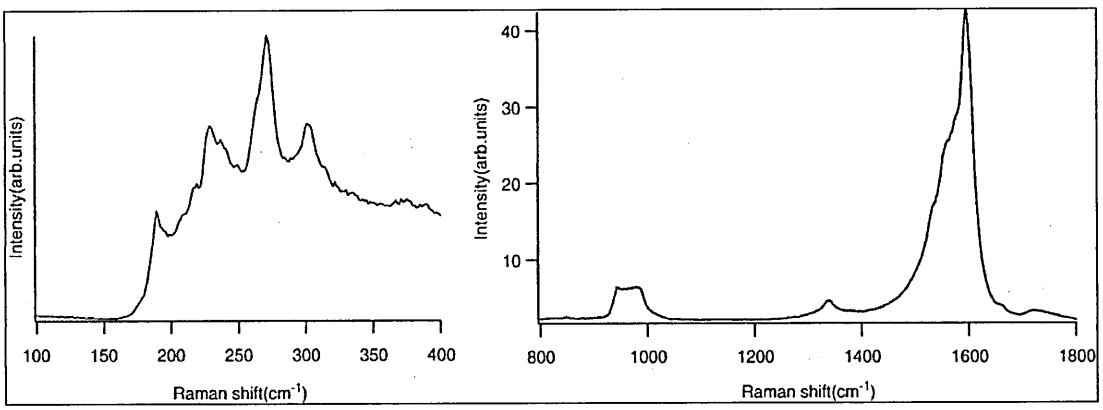

Figure 2. Raman spectra of as-grown SWCNTs from dip coating

In another study, we varied the dipping time of silicon substrates inside the solution at 80°C from 10 minutes to 5 hours. Fig. 3 is the SEM images of carbon nanotubes obtained in this case. Dipping for a longer period left large amount of catalyst particles on the substrates. Fig. 3(a) shows the emergence of CNTs from cracked part of catalyst after complete drying of the solution. Fig. 3(b),(c),(d) are the SEM images of CNTs obtained after dipping time of 2 h, 1 h and 20 min respectively. It suggests that density of catalyst particles and diameter of nanotubes reduce in shorter dipping time. Evaporation rate of ethanol is found to be 1.7% in every 30 min at 80 °C.

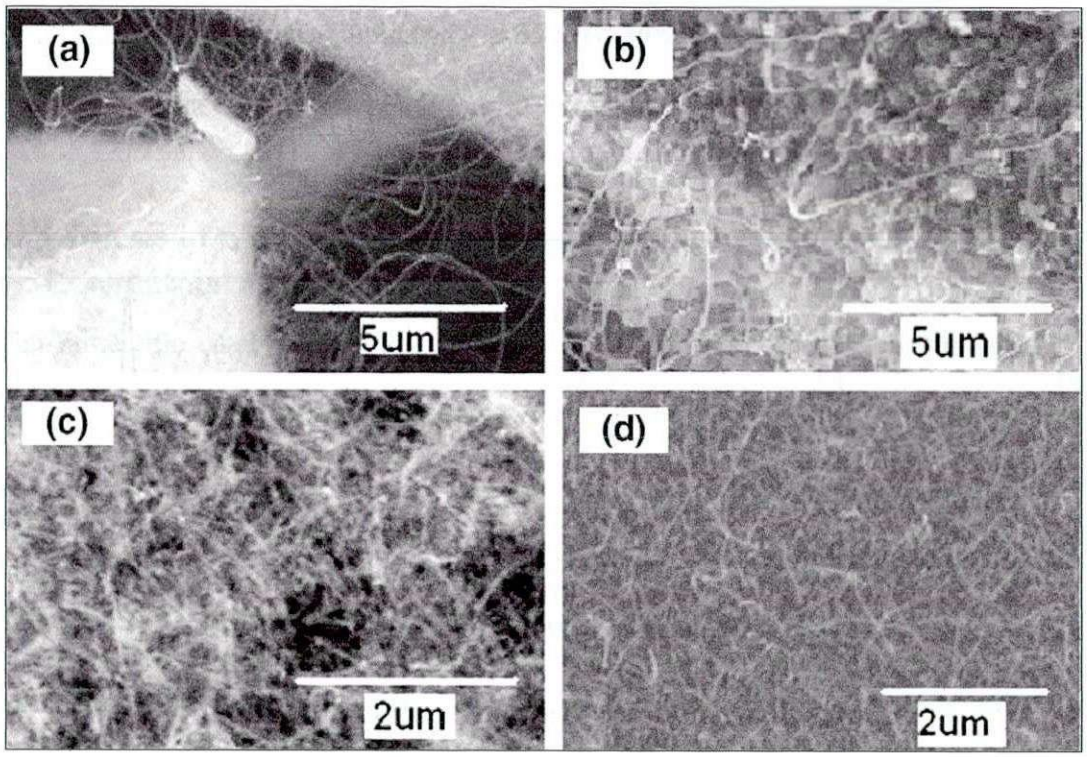

Figure 3. SEM images of CNTs synthesized at different interval of dipping time (a) complete drying of the solution (b) 2 h (c) 1 h and (d) 20 min.

Larger diameter of the nanotubes in longer dipping time were also observed from TEM images. Agglomeration of the catalyst particles is higher in longer dipping time, this may be the reason for the large diameter of CNTs. Fig. 4(a) is a TEM image of as grown CNTs after dipping time of 5 h. Nanotubes of smaller diameter were obtained in shorter dipping time. Fig. 4(b), (c) are the TEM images of CNTs after 2 h and 20 min dipping time. Interestingly in 20 min dipping time, Raman spectra of SWCNTs were also observed. Fig. 3(d) shows surface morphology of CNTs obtained in silicon substrate. TEM image of this sample indicates the presence of SWCNTs (shown by arrow) in Fig. 4(c). Growth of SWCNTs might have been happened because a suitable concentration of catalyst for its formation has been mounted on substrates. Furthermore, in 10 min dipping, Raman spectra of SWCNTs were found easily. Fig. 4(d) clearly

shows the presence of SWCNTs. We tried with different wt.% of catalysts. In every experiments, Raman spectra of SWCNTs were obtained easily.

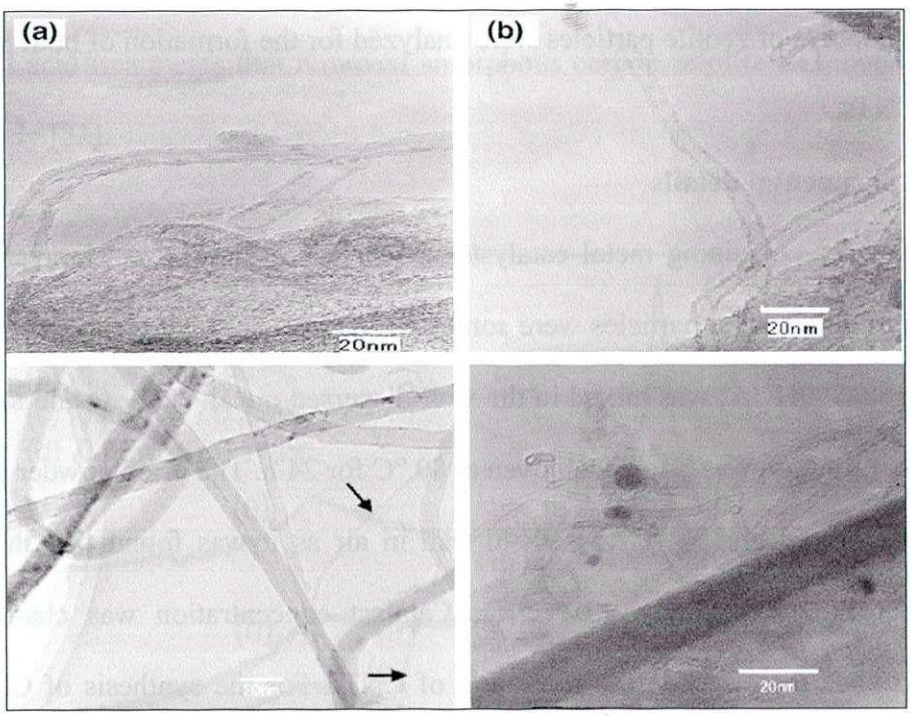

Figure 4. TEM images of as synthesized CNTs at different dip coating time (a) 5 h (b) 2 h (c) 20 min (d) 10 min.

2.3.3. Summary

In this work, we presented a method of synthesizing SWCNTs by ultrasonic spray pyrolysis method in nitrogen environment without using vacuum pump and reducing agent in a simple set up. It is believed that comparative study of drying of substrates inside catalyst solutions at different time show the role of formation of SWCNTs and MWCNTs. Large agglomerates of metal catalysts are the result of longer dipping time, which produces MWCNTs of larger diameter. Similarly, shorter dipping time mount smaller metal catalysts on the substrates that produces SWCNTs of smaller diameter.

2.4 Synthesis of CNTs on zeolite supporting material

The system is also analyzed with zeolite supporting material for the synthesis of CNTs in large quantity [14]. The important roles played by catalyst concentration, flow rate of gas and nanopores of zeolite particles were analyzed for the formation of both SWCNTs and MWCNTs.

2.4.1. Experimental details

Zeolite powder containing metal catalysts was prepared similar to Maruyama et al. [21]. First of all, catalyst particles were sonicated in ethanol for an hour. Y-type zeolite powder [HSZ-390HUA] was mixed in the well-dispersed metal catalysts and stirred for 2–3 h. The solution was dried in an oven at 80 °C for 24 h. The dried powder was then grinded and heated at 350 °C for 30–40 min in air as it was found that this initial heating increases the yield of SWCNTs. Catalyst concentration was changed and examined to see the effect in the formation of CNTs. For the synthesis of CNTs, the powder was placed in the middle of the quartz tube and both the ends were closed by quartz joints with the nebulizer on one side and a water bubbler on the other side. Nitrogen gas flow was kept constant at 2.0 l/min until the set temperature was reached. When the reaction furnace reached the set temperature, N2 gas flow was increased to 2.5 l/min and let flowing for 5 more minutes. Carbon mist was produced inside atomization chamber and carrier gas passed this mist into the furnace.

2.4.2 Results and discussion

Fig. 5 shows Raman spectra of CNTs synthesized at different weights % of Fe and Co acetate at 850 °C in nitrogen flow rate of 2.5 l/min. It is characterized by G and D peaks. The G-peak appears ataround 1598 cm^{-1} and is ascribed to tangential modes of a graphene sheet. The D-peak at around 1328 cm^{-1} is related to the defects in a graphene sheet and presence of amorphous carbon. We tried different alloy of transition metal

particles on zeolite but alloy of Fe/Co particles showed better results. It is cleared from Raman spectra that crystallinity and quality of CNTs (Ig/Id ratio) decreases with increasing Fe concentration. As-grown CNTs materials were purified by annealing, alkali and acid treatments that removed amorphous carbon, zeolite and metal particles respectively [22].

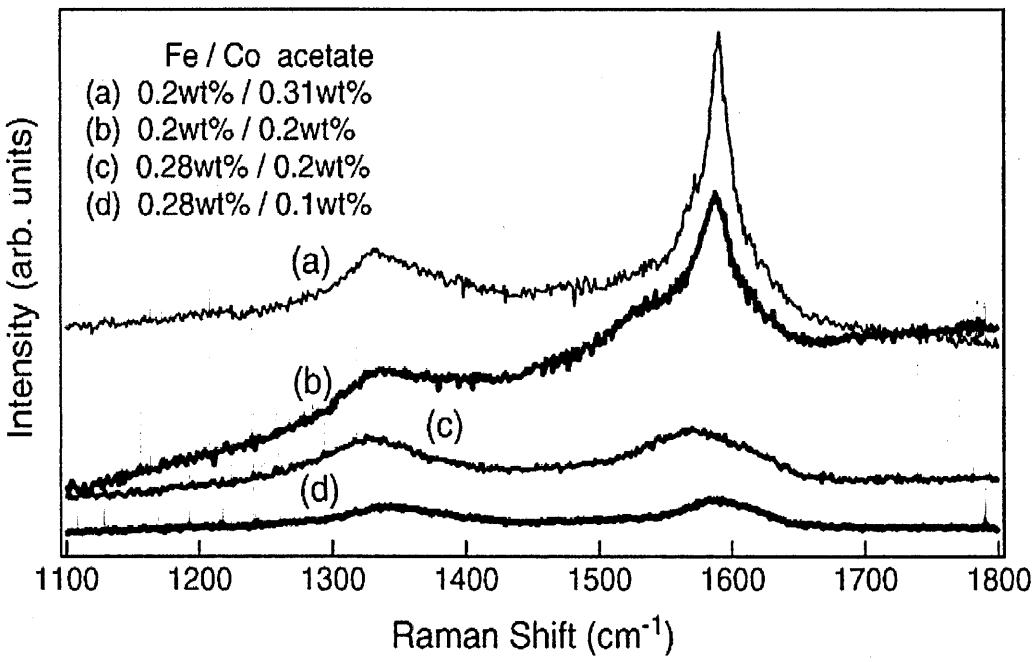

Figure 5. Raman spectra of as-grown CNTs synthesized at different weights % of Fe-Co in zeolite supporting material.

Figure 6 shows TEM image of SWCNTs obtained at 0.2 wt.% of iron acetate and 0.3 wt.% of cobalt acetate in 50 ml of ethanol solution. In TEM observation, a few amounts of MWCNTs were also examined but the dominating yield was SWCNTs. As it is conform from TEM images that SWCNTs yield were about 68+(−)5%. In other concentration, SWCNTs were not obtained easily and only iron catalyst did not produce

SWCNTs. Previous works performed on different system also showed similar results [23,24]. Generally, metal oxide particles change into metal particles by reducing agent [25] or reducing carbon sources [26,27] for the formation of SWCNTs. However, our system does not have any reducing agent or reducing carbon sources. So, the sizes of metal particles interaction with nanopores of zeolite are key factors to determine the formation of SWCNTs.

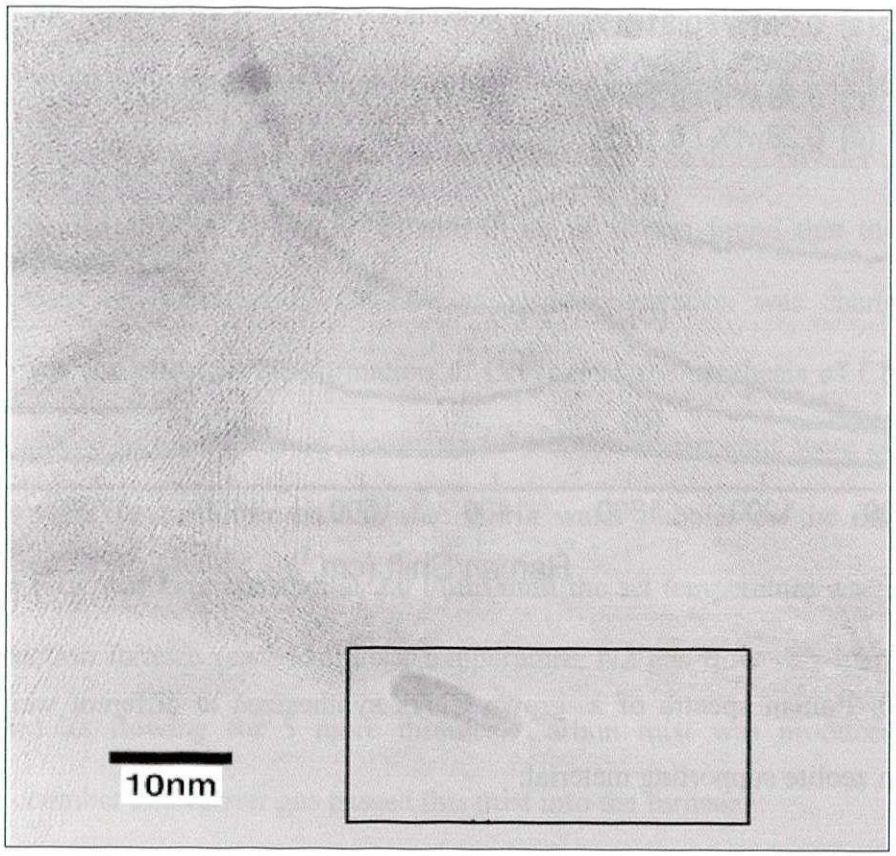

Figure 6. TEM image of SWCNTs and marked spot shows MWCNTs.

2.4.3 Nanotubes growth mechanism on zeolite

Zeolite [14,22,29] and zeolite like supporting materials (MCM41) [24,30,31] are extensively used for synthesis of SWCNTs. In equal wt.% of Co and Fe catalyst, we obtained both SWCNTs and MWCNTs in same amount. It is expected that a small

amount of other element present in zeolite (like aluminium (Al)) can alter the chemical properties of SiO_2 framework. For example, Palanisamy et al. used Al–MCM41 and zeolite to study the effect of Al during nanotube growth [24]. They obtained identical result with both of the materials, which yield MWCNTs. In acetylene CVD, it was conformed from X-ray photoelectron spectroscopy (XPS) that Al alters the chemical state of Fe [26 and therein]. At present, we are not focusing on the chemical status of the catalyst and we are not using any hydrocarbon, reducing agent to grow CNTs. However, we believe that concentration and interaction of catalyst particles to zeolite are the key factors to form CNTs. It is suggested that zeolite contains well-ordered, nanometer-sized void spaces (ca. 3–15A) in structures [32]. To examine such behaviors and nanopores, we took different TEM images of zeolite particles. TEM image in Fig. 7(a) shows the well-ordered nanopores (right hand side) and deformed spots (left hand side) of the same zeolite particle. We don't know the clear reason for such deformed spots. It should be either created from electron beam irradiation during TEM observation while trying to bring the camera into focus or some chemical interaction of catalyst to zeolite. Similarly, Fig. 7(b) shows large metal particles on the zeolite substrate. In some TEM images, we obtained SWCNTs of large diameter. Such SWCNTs might have been grown from agglomerated metal particles but not from metal catalyst encapsulated in nanopores of zeolite. Likewise, when nucleation of carbon triggered in larger metal particles,MWCNTs would form. Fig. 7(c) shows TEM image of MWCNTs emerged from the zeolite particle.

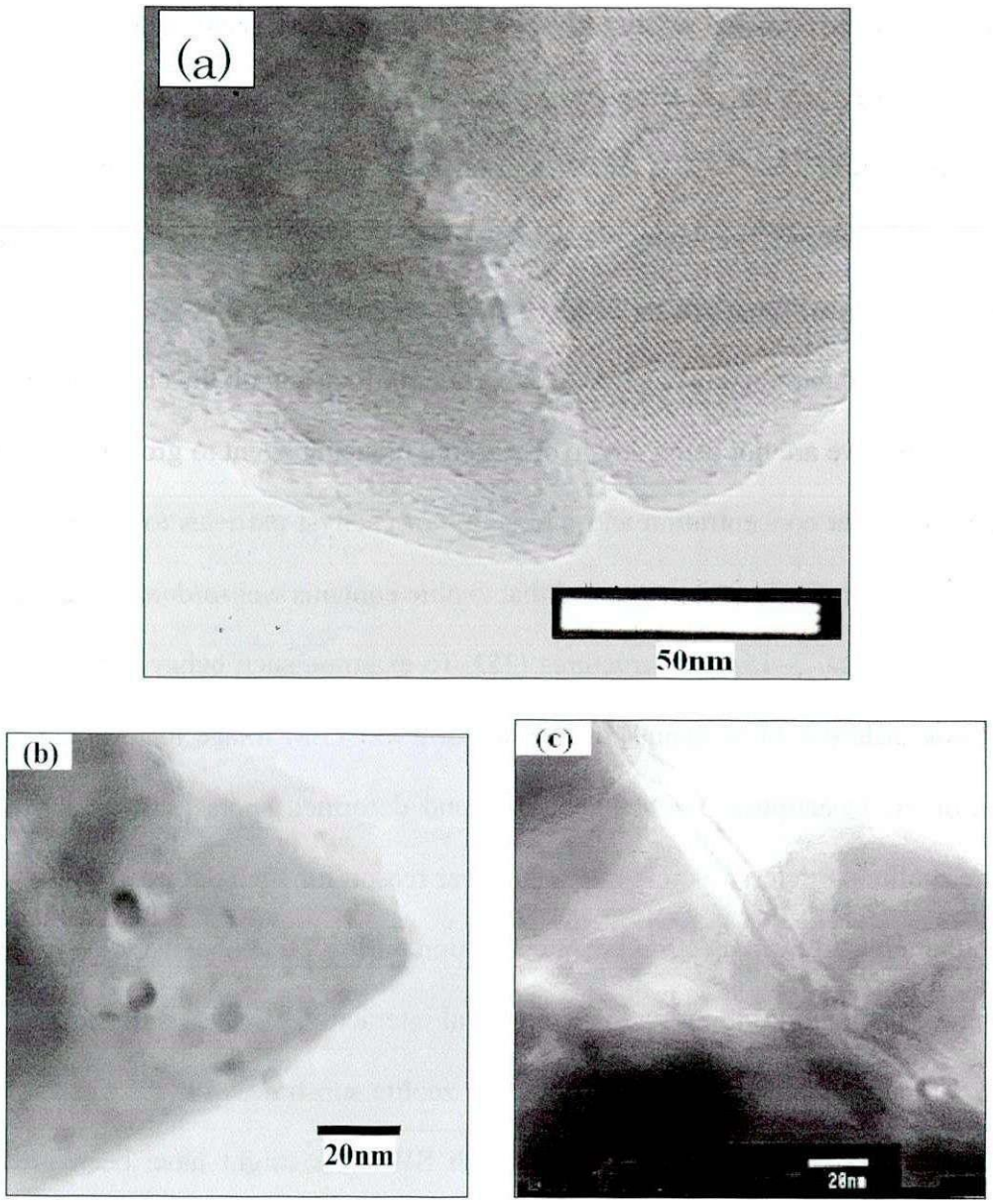

Figure 7 (a) Well-ordered nanopores (right hand side) and deformed spots (left handside) of the same zeolite particle. (b) TEM image of metal encapsulated zeolite particles. (c) MWCNTs observed on the surface of zeolite particle.

So, it can be said that small metal particles encapsulated in zeolite or metal particles on the nanopores surface of zeolite produce SWCNTs whereas agglomerated large metal particles produce MWCNTs. Furthermore, Fig. 8(a) and (b) show the highly-magnified images of MWCNTs formed on large metal catalyst. It is said that when nucleating is triggered, the carbon-saturated catalyst particle precipitates its carbon on metal catalyst and the number of nucleation caps formed will depend on the catalyst volume to surface area ratio [33]. It means larger metal cluster precipitates much carbon. Fig. 8(a) and magnified selection portion of Fig. 6 in Fig. 8(b) show "ice-cream cone" terminated MWCNTs. Pentagons and heptagons carbon rings play a key role in the tube-tip shapes [29]. These CNT seem to be accelerated from tip end of metal catalyst. Hence, it can be assumed that in shaped metal catalyst nucleation of a CNTs cap occurs dominantly to the forward direction.

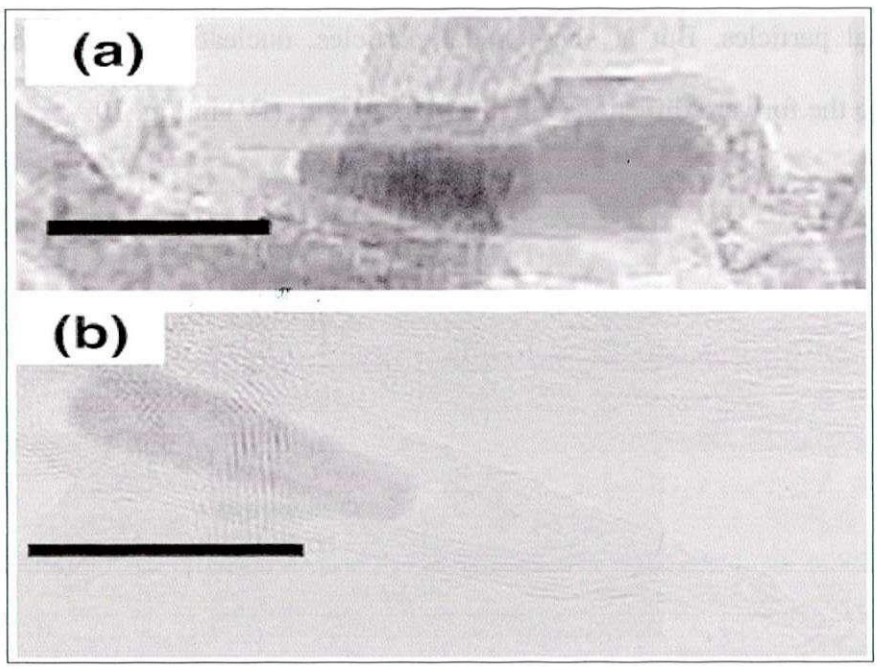

Figure 8. MWCNTs elongated from the sharp side of metal catalyst. (b) Tip of MWCNTs terminated with defects. Scale bar is 10nm in each figure

Hence, the growth processes of CNTs on zeolite are summarized as follows.

(a) SWCNTs originate from metal particles located on the surface of nanopores of zeolite. We observed metal particle at the tip and root of the CNTs [(Fig. 9(a) and (b)], which suggest that both tip and root growth mechanism coexist. Marked with (I) in Fig. 10.

(b) SWCNTs of larger diameter do not originate from metal particles located on the surface of nanopores of zeolite but they originate from agglomerated small metal catalyst. Likewise, MWCNTs originate from large metal catalyst [Fig. 7(b) and (c)]. Marked with (II) in Fig. 10.

(c) Metal particles were often observed inside the MWCNTs, indicating the weak metal–support interaction in zeolite [Fig. 9(c)]. Marked with (III) in Fig. 10.

(d) In some cases, metal catalyst precipitates carbon and forms carbon layers all around the metal particles. But at sharp metal particles, nucleating of a nanotubes cap occurs to the forward direction (Fig. 8). Marked with (IV) in Fig. 10.

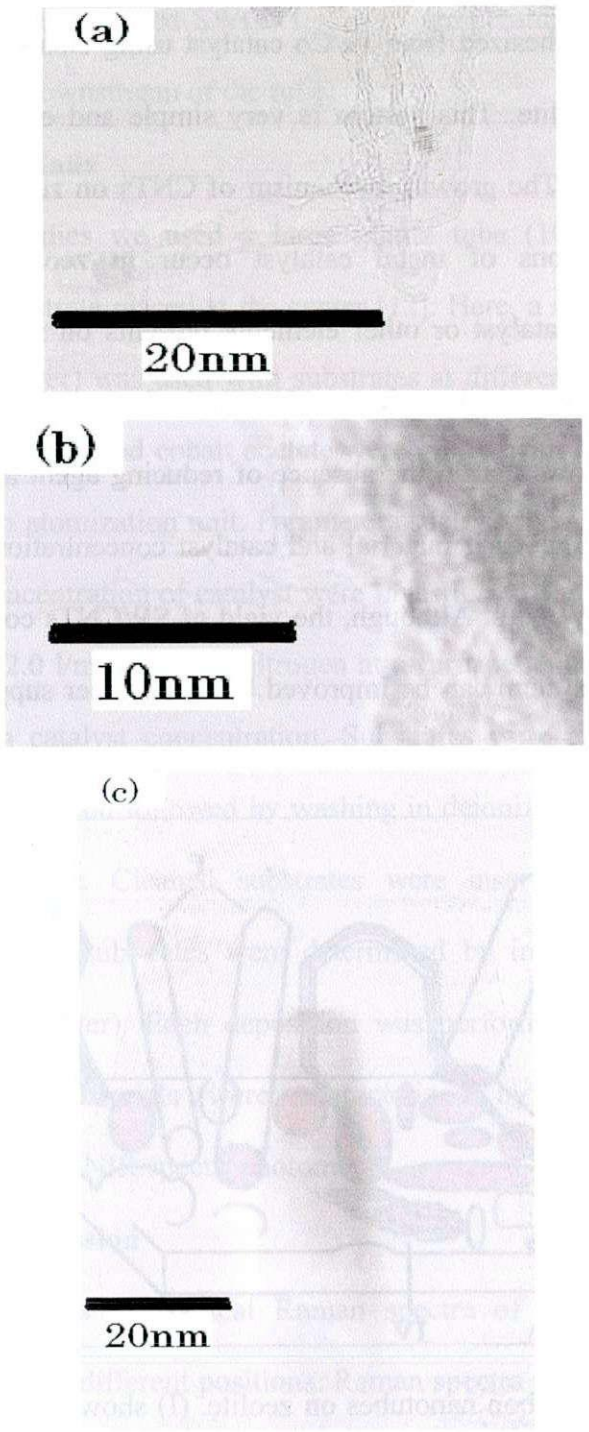

Figure 9 (a) Tip and (b) base growth of CNTs on zeolite particles. (c) Metal particles trapped inside the MWCNT.

2.4.4 Summary

SWCNTs were synthesized from Fe/Co catalyst using ethanol byultrasonic spray pyrolysis method in zeolite. This system is very simple and ease of scaling into an industrial scale process. The growth mechanism of CNTs on zeolite was studied. We found that agglomerations of metal catalyst occur in zeolite either by higher concentration of metal catalyst or other elements presents on it. MWCNTs generate from these large catalyst particles whereas SWCNTs from smaller catalyst particles. The present method shows that in the absence of reducing agent and reducing carbon source, nanopores of supporting material and catalyst concentration play crucial roles for the formation of SWCNTs. Although, the yield of SWCNTs contain a few amount of MWCNTs, but this system can be improved by using other supporting material for large-scale production.

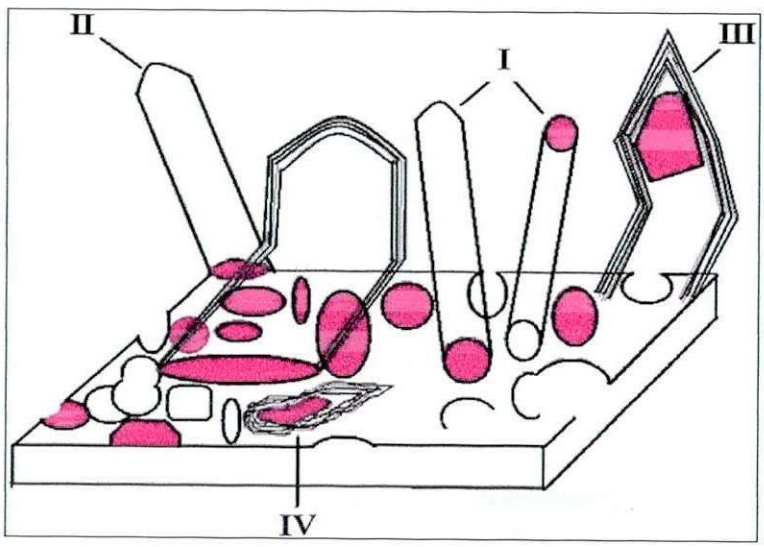

Figure. 10 Growth of carbon nanotubes on zeolite. (I) shows base and tip growth of SWCNTs. (II) shows SWCNTs generated from encapsulated metal particles. (III) shows weak interaction of metal catalyst with supporting materials. (IV) shows directional growth of MWCNTs in metal catalyst.

CHAPTER 2
SYNTHESIS OF CARBON NANOTUBES BY ULTRASONIC SPRAY PYROLYSIS

2.5 Simultaneous formation of both SWCNTs and MWCNTs

In this work, we collected SWCNTs at low temperature on desire substrate by placing the substrates downstream of the tube.

2.5.1 Experimental details

In our previous studies we used a large quartz tube (100 cm long and 75mm diameter) with the substrate placed at the center [12]. Here, a small quartz tube (55 cm long and 25mm diameter) was used with substrates at different positions, as shown in Fig. 11(a). Here, ferrocene and cobalt acetate were mixed with ethanol and placed in a medication cup in an atomization unit. Parameters such as the reactor temperature, gas flow, and relative concentration of catalyst were investigated and adjusted. We obtained good results with a 2.0 l/min flow of nitrogen at a furnace temperature of 1000°C and 0.032 wt% for each catalyst concentration. Substrates were cleaned in acetone and methanol by ultra sonication followed by washing in deionized water, and finally dried using a nitrogen blower. Cleaned substrates were inserted inside the tube. The temperatures around the substrates were determined by inserting thermocouple (AS ONE TM-300 thermometer). Each deposition was performed for 15 minutes. After deposition, as-grown materials were characterized by SEM, TEM, Raman spectroscopy and UV/vis/ NIR spectrophotometry.

2.5.2 Results and discussion

Fig 11 (b) represents the typical Raman spectra of CNTs formed on silicon substrates placed at three different positions. Raman spectra at positions 2 and 3 appear with the radial breathing mode (RBM) at a low wave number. The RBM peak of SWCNT at position 2 appears at 150, 222, and 263 cm^{-1}, which correspond to the SWCNTs diameters of 1.65, 1.117, and 0.94 nm, respectively. The RBM peak of substrates at position 3 shows SWCNT diameters of 1.35, 1.08, and 0.93 nm,

respectively. The diameter of the nanotube is expected to reflect the size of the catalytic particle at the time of tube nucleation. Thus, it can be predicted that the size of catalyst particles responsible for forming SWCNTs on position 2 are slightly larger than catalyst particles on position 3. This may be because some catalyst particles remain under a floated condition, which causes the decomposed carbon source to dissolve and form SWCNTs at high temperature in floated condition. Thus, lighter SWCNTs traveled longer distances and accumulated downstream of the tube, whereas metal catalysts at the center of the tube accumulate to form large metal catalyst that make MWCNTs. Khavrus et al. also proposed a similar growth mechanism for the simultaneous growth of nitrogen doped SWCNTs and MWCNTs [34].

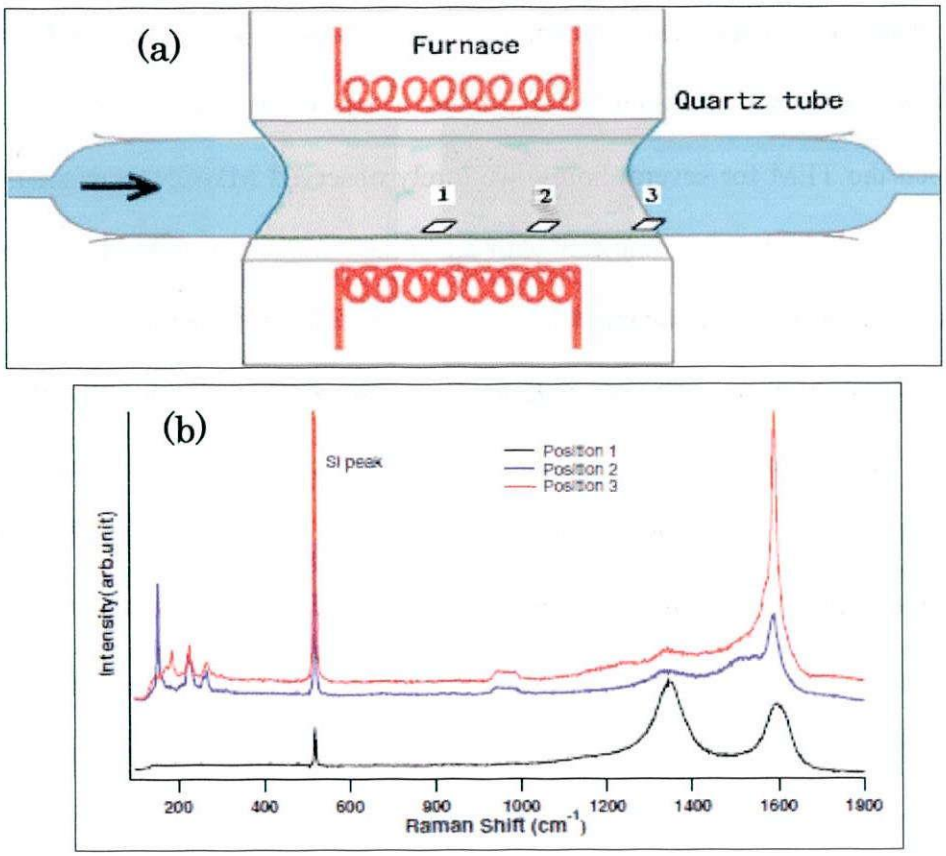

Figure 11 (a) Schematic diagram of the reactor and the position of substrates inside the quartz tube. (b) Typical Raman spectra of as-grown CNTs on silicon substrates on different position (i) center of the tube (ii) 7cm, and (iii) 14cm, from the midpoint of the furnace.

Here, ethanol/catalyst particle mist passes through a high-temperature (1000°C), creating enough opportunities for small catalyst particles to nucleate under the floating condition. In the next step, the silicon substrate at position 3 was replaced by FTO substrates. Thermocouple measurement shows the temperature around position 3 to be below 300°C. Figures 12(a) and 2(b) show the SEM images of MWCNTs and SWCNTs formed on silicon and FTO substrates at positions 1 and 3, respectively. In clear observation, one can notice the surface of FTO at the back in Fig. 12(b), which confirm that there are no cracks and the temperature is low. The insets show respective TEM

images of the samples. Dense bamboo-structured MWCNTs were formed on the silicon substrates, whereas pure SWCNTs were observed on FTO substrates. As we carefully scanned the TEM for several hours, we rarely observed MWCNTs. A small bundle of SWCNTs of about 1 nm diameter with clean tube walls were observed. Increasing the ferrocene concentration enhances the yield of SWCNTs at position 3, along with a large number of non-nucleated metal particles. However, only cobalt acetate produces fewer SWCNTs, and ferrocene only produces large carbon impurities. Raman spectroscopy was used to analyze the purity of materials so formed. Figures 12(c) and 12(d) show the Raman spectra of MWCNTs obtained on silicon and FTO substrates, respectively. At position 1, G- and D-band intensities become almost the same. The reason for this may be the disordered graphene sheets of MWCNTs, as observed in the inset of Fig. 12(a). In comparison, the well-known RBM, the D- and G-bands were observed on FTO substrates. As a reference, the bottom spectrum in Fig. 12(d) was measured from FTO substrates only. The FTO substrate shows some peaks at a lower wave number. In Raman spectra in Fig. 12(d), we can see some additional peaks of SWCNTs. At position 3 several substrates, including ITO, FTO, metallic, semiconductor, insulator, and plastic were placed and tested. SWCNTs were formed in all cases.

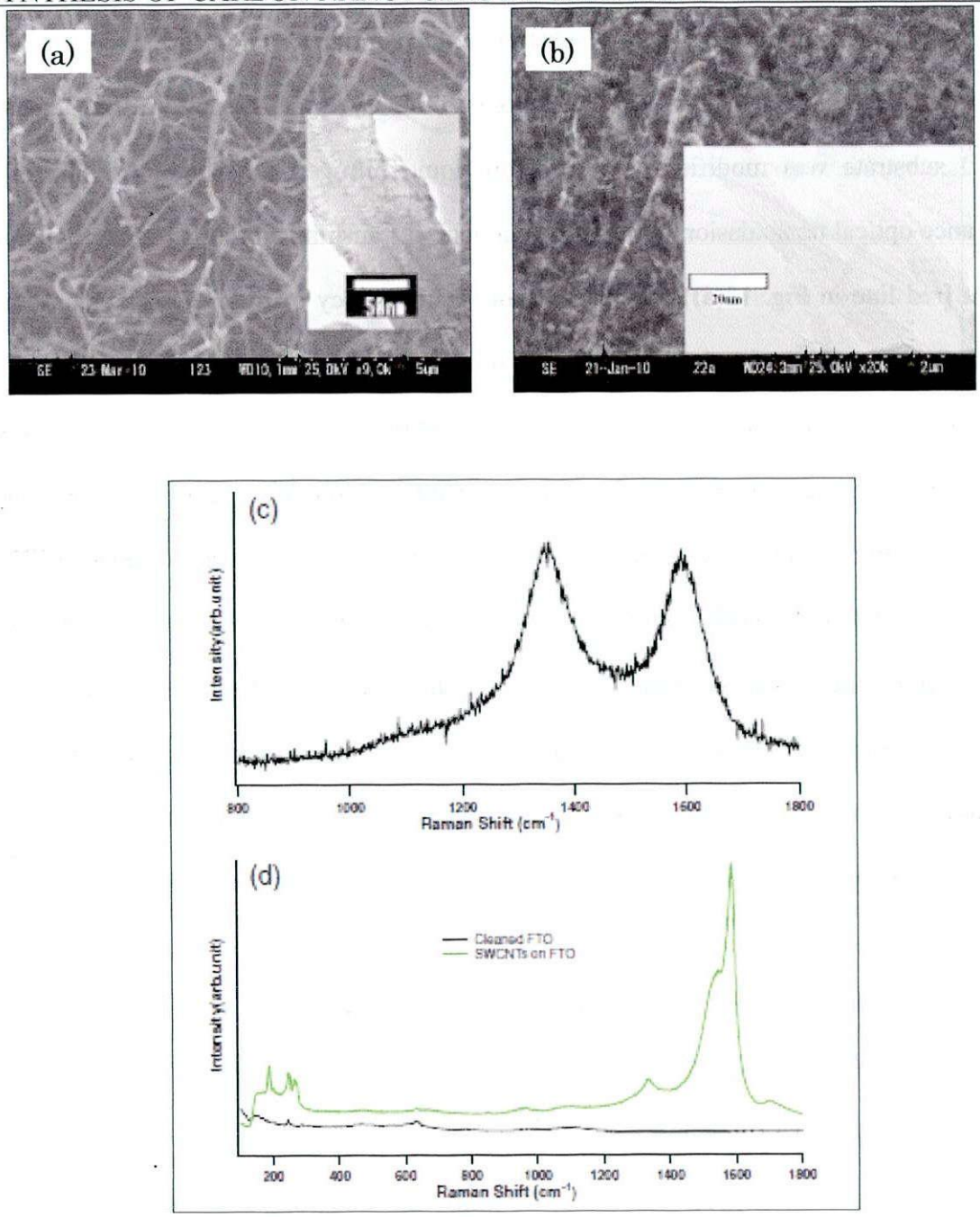

Figure 12. SEM image of (a) MWCNTs and (b) SWCNTs formed at center and downstream of the tube. Insets show the corresponding TEM images. Raman spectra of (c) MWCNTs and (d) SWCNTs obtained on silicon and FTO substrates.

Light transmission of the FTO substrate reduced after SWCNT formation. But we performed liquid nitrogen and ozone treatment to improve transparency. At first, a clean FTO substrate was modified by boiling in liquid nitrogen for 5 min (LNFTO) to enhance optical transmission. After this treatment, it transmits more than 95% of visible light [red line in Fig. 13(a)] around 800 nm. Transparency of the FTO substrate is an important parameter in the performance of solar cells. Recently, Afre et al. [35] performed a similar treatment to enhance the performance of organic solar cells. The light transmission of LNFTO decreased after SWCNT formation and reached around 60% [blue line in Fig. 13(a)] at 800 nm. Then, the substrate was treated for about 1 hour in a UV/vis/NIR spectrophotometer for ozone oxidation [green line in Fig. 13(a)]. This treatment brings its transparency back to its original state of FTO substrate. It has been suggested that short exposure (<20 min)) to ozone introduces defects that increase the catalytic activity of the nanotubes without significantly changing either the light transmission or sheet resistance. Longer exposure begins to degrade tubes, increases the transmittance, sheet resistance, and charge transfer resistance [36]. Figure 13(b) and 13(c) show SEM images of the SWCNT film on LNFTO before and after ozone treatment. Note the network of SWCNTs on the surface, it disappeared upon ozone oxidation of 1 h. The remaining SWCNTs might have been oxidized into ethers or epoxides and carbonyls [37], which may be important for strong interaction with other semiconducting materials such as titanium dioxide or organic polymer in optoelectronic application.

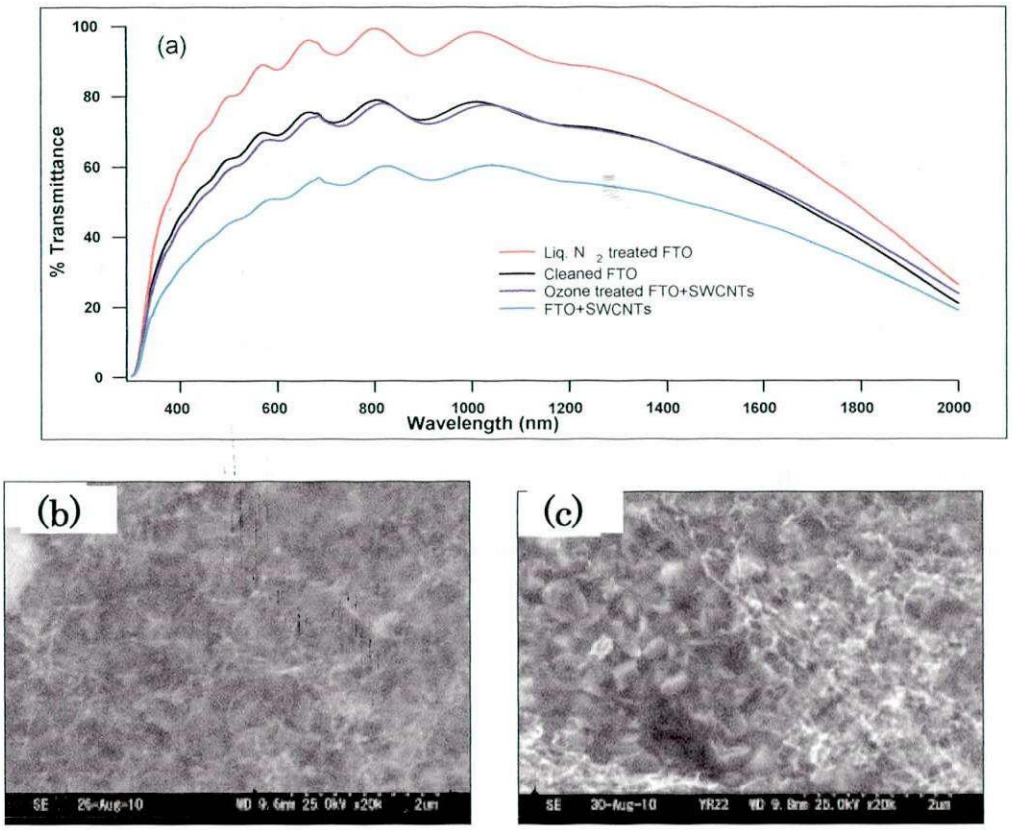

Figure 13 (a) Optical transmission spectra of SWCNTs on FTO substrate, (b) SEM image of SWCNTs on LNFTO substrate, (c) SEM image of SWCNTs on LNFTO after 1 h of ozone treatment.

2.5.3 Summary

We passed a mist of ethanol/catalyst particles through a high temperature of the furnace with the substrate placed downstream of the tube at low temperature. Raman, SEM and TEM measurements show the simultaneous formation of MWCNTs and SWCNTs. We believe that catalyst particles in the hot region agglomerate to form a large metal catalyst, and MWCNTs were formed. At the same time, floating catalyst particles dissolve the carbon source and become nucleated under the floated condition to form SWCNTs that passes through carrier gas to downstream of the tube. Finally, we

measured the transparency of SWCNTs grown on FTO substrates with the aim of using them in various optoelectronic devices. The transparency of the SWCNT–FTO substrate decreases after SWCNT formation but returns to its initial stage after ozone treatment.

2.6 Conclusion

In this chapter, we demonstrated the synthesis of both SWCNTs and MWCNTs on different substrates and zeolite supporting material by ultrasonic spray pyrolysis method. This system is very simple and easy to handle, which doesn't require any reducing agent and vacuum pump for the synthesis of carbon nanomaterials.

CHAPTER 2
SYNTHESIS OF CARBON NANOTUBES BY ULTRASONIC SPRAY PYROLYSIS

References:

[1] C. Journet, W.K. Maser, P. Bernier, A. Loiseau, M.L. de la Chapelle, S. Lefrant, P. Deniard, R. Lee, J.E. Fischer, Nature 388 (1998) 756.

[2] K.S. Subrahmanyam, L.S. Panchakarla, A. Govindaraj, C.N.R. Rao, J. Phys. Chem. C, 113 (2009) 4257

[3] M. Pacheco, J. Pacheco, R. Valdivia ISBN 978-953-7619-88-2 pp. 438, (2010) Nanofibers, Publisher InTech

[4] T. Guo, P. Nikoleav, A. Thess, D.T. Colbert, R.E. Smalley, Chem. Phys. Lett. 243 (1995) 49.

[5] E. Cappelli, S. Orlando, V. Morandi, M. Servidori, C. Scilletta. J. Phys.: Conf. Ser., 59 (2007) 616.

[6] Y. Suda, A. Tanaka, A. Okita, Y. Sakai, H. Sugawara, J. Phys.: Conf. Ser., 59, 348

[7] R. Kamalakaran, M. Terrones, T. Seeger, Ph. Kohler-Redlich, M. Ruhle, Y.A. Kim, T.Hayashi, M. Endo, Appl. Phys. Lett. 77 (2000) 3385.

[8] A. N. Obraztsov, Nature Nano. 4 (2009) 212.

[9] G. Che, B.B. Lakshmi, C.R. Martin, E.R. Fisher, R. S. Ruoff. Chem. Mater. 10 (1998) 260.

[10] S. Maruyama, R. Lojima, Y. Miyauchi, S. Chiashi, M. Kohno, Chem. Phys. Lett. 360 (2002) 229.

[11] Y. Miyata, K. Kamon, K. Ohashi, R. Kitaura, M. Yoshimura, H. Shinohara. Appl. Phys. Lett. 96 (2010) 263105

[12] I. Khatri, T. Soga, T. Jimbo, S. Adhikari, H.R. Aryal, M. Umeno, Diamond Relat. Mater. 18 (2009) 319.

[13] S. M. Mominuzzaman, I. Khatri, Z. Jianhui, T. Soga, T. Jimbo, IEEE (2008) 249.

[14] I. Khatri, N. Kishi, T. Soga, T. Jimbo, S. Adhikari, H. R. Aryal, M. Umeno, Thin Solid Films, 518 (2010) 6756.

[15] J. Zhang, I. Khatri, N. Kishi, T. Soga, T. Jimbo, IEICE TRANS.ELECTRON., E92-C (2009) 1432.

[16] J. Zhang, I. Khatri, N. Kishi, T. Soga, T. Jimbo, Materials Letters, 64 (2010) 1243.

[17] J. Zhang, I. Khatri, N.Kishi, T. Soga, T. Jimbo, Thin solid Films, 519 (2011) 4162.

[18] I. Khatri, N. Kishi, J. Zhang, T. Soga, T. Jimbo, Jpn. J. Appl. Phys. 50 (2011) 020213.

[19] Y. Murakami, Y. Miyauchi, S. Chiashi, S. Maruyama, Chem. Phys. Lett. 377 (1-2) (2003) 49.

[20] R. Saito, G. Dresselhaus, M.S. Dresselhaus, Phys. Rev. B 61 (2000) 2981.

[21] S. Maruyama, R. Lojima, Y. Miyauchi, S. Chiashi, M. Kohno, Chem. Phys. Lett. 360 (2002) 229.

[22] S. Okubo, T. Sekine, S. Suzuki, Y. Achiba, K. Tsukagoshi, Y. Aoyagi, H. Kataura, Jpn. J. Appl. Phys. 43 (2004) L396.

[23] S. Inoue, Y. Kikuchi, Chem. Phys. Lett. 410 (2005) 209.

[24] P. Ramesh, N. Kishi, T. Sugai, H. Shinohara, J. Phys. Chem. B 110 (2006) 130.

[25] A.R. Biris, Z. Li, E. Dervishi, D. Lupu, Y. Xu, V. Saini, F. Watanabe, A.S. Biris, Phys. Lett. A 372 (2008) 3051.

[26] Y. Homma, Y. Kobayashi, T. Ogino, D. Takagi, R. Ito, Y.J. Jung, P.M. Ajayan, J. Phys.Chem. B 107 (2003) 12161.

[27] H. Ago, K. Nakamura, N. Uehara, M. Tsugi, J. Phys. Chem. B 14 (2004) 18908.

[28] T. Hayashi, Y.A. Kim, T. Matoba, M. Esaka, K. Nishimura, T. Tsukada, M. Endo, M.S. Dresselhaus, Nano Lett. 3 (2003) 887.

[29] S. Iijima, T. Ichihashi, Y. Ando, Nature 356 (1992) 776.

[30] P.B. Amama, S. Lim, D. Ciuparu, Y. Yang, L. Pfefferle, G.L. Haller, J. Phys. Chem. B 109 (2005) 2645.

[31] D. Ciuparu, Y. Chen, S. Lim, G.L. Haller, L. Pfefferle, J. Phys. Chem. B 108 (2004) 503.

[32] T. Wakihara, T. Okubo, Chem. Lett. 34 (2005) 276.

[33] M.H. Rummeli, C. Kramberger, M. Loffler, O. Jost, M. Bystrzejewski, A. Gruneis, T.Gemming, W. Pompe, B. Buchner, T. Pichler, J. Phys. Chem. B 111 (2007) 8234.

[34] V. O. Khavrus, E. M. M. Ibrahim, A. Leonhardt, S. Hampel, S. Oswald, C. Taschner, and B. Buchner: J. Phys. Chem. C 114 (2010) 843.

[35] R. A. Afre, Y. Hayashi, and T. Soga: J. Phys. D 42 (2009) 042002.

[36] J. E. Trancik, S. C. Barton, and J. Hone: Nano Lett. 8 (2008) 982.

[37] D. B. Mawhinney, V. Naumenko, A. Kuznetsova, J. T. Yates, Jr., J. Liu, R. E. Smalley: J. Am. Chem. Soc. 122 (2000) 2383.

CHAPTER 3

POLYMER SOLAR CELL USING CARBON NANOTUBES

CHAPTER 3
POLYMER SOLAR CELL USING CARBON NANOTUBES

The semiconducting polymer thin film has gained substantial interest in the research community because of the possibility to produce polymer based photovoltaic devices by roll to roll type manufacture, which is impossible by conventional technologies. Hole transferring semiconducting polymer and electron accepting fullerene (C_{60}) derivative are of special interest because of their stability and high power conversion efficiencies. With the discovery of new carbon "carbon nanotubes" (CNTs), researchers have started blending them with polymer for improving the solar cell efficiency. CNT incorporated solar cell shows better power conversion efficiency than pristine solar cell without CNTs. This is because of the wonderful properties of CNTs. CNTs have outstanding properties like ballistic conductive, high aspect ratio, high surface area, flexible, strong, rigid, environmental stable, capability of charge dissociation, transportation and so on, which are believed to be an ideal material for fabricating high performance solar cell.

CHAPTER 3
POLYMER SOLAR CELL USING CARBON NANOTUBES

3.1 Introduction

A solar cell converts sunlight into electricity directly through the photovoltaic (PV) effect. In semi-conducting material electrons live in range of define energy level called band. The conduction band is partially filled with electrons, creating negative charge. The valance band has areas where electrons are missing known as hole (positive charge). In the absence of light, the positive and negative charges balance each other in the case of intrinsic semiconductors. When light energy strikes on semiconductor p-n junction, the electrons are dislodged causing electrons to move down an external circuit in the form of light-generating electricity. This phenomenon is called PV effect. Detail theoretical description is given in ref [1]. If light with photon energy is greater than optical band gap, free electrons and free holes are formed by optical excitation in the semiconductor. Different materials used for solar cells are: Silicon (Si), Copper indium gallium selenide [$Cu(In,Ga)Se_2$], Cadmium Sulfide (CdS), Cadmium Telluride (CdTe), Titanium dioxide (TiO_2) etc. Silicon and compound semiconductor based devices are dominating solar technology. However, the cost of these solar cells is much high to reach for daily life. So, low cost and high efficiency solar cells are yet to be realized for their commercialization. In the search for alternative material, carbon is highly attractive because it is expected to have similar properties to silicon and it is highly stable. Carbon is a remarkable element that exist in a variety of forms ranging from insulator/semiconducting diamond (or diamond-like amorphous film [2]) to metallic/semi-metallic graphite (or graphene [3]), conducting/semiconducting fullerenes (e.g. C_{60} [4]) and carbon nanotubes (CNTs) [5]. On the other hand, the organic polymer-based materials are promising too because of their high manufacture using roll to roll or spray deposition. Attractive additional features are the possibilities to fabricate flexible devices, which can be integrated into curved surfaces, existing building

structure. Furthermore, the polymer–CNTs composite materials have potential macroscopic device application, such as light-emitting diodes (LED), field-effect transitions (FET) and PV devices [6–9].

3.2 Organic semi-conducting materials and carbon nanotubes

Organic semi-conducting materials exist either in small size of small molecules with molecular weight of less than a few thousand atomic mass units (amu), or polymer with molecular greater than 10,000 (amu). Semi-conducting donor like organic polymer such as poly (3-hexylthiophene) (P3HT), poly [2-methoxy-5-(20-ethyl-hexyloxy)-1,4-phenylene vinylene] (MEH-PPV), poly(3-octylthiophene) (P3OT) are derivative of phenylene vinylene, thiophene chain. They can be doped chemically, photochemically or electrochemically methods. The merits of organic semi-conductor materials are

1. They show high absorption coefficients exceeding 10^5 cm^{-1} [10]
2. Electronic band gap can be engineered by chemical synthesis [11]
3. Block polymer composition can be designed in such a way that one block of polymer can interacts with third compounds (like quantum dots, quantum wires) while the other block(s) improve solubility [12]
4. Charge carrier mobilities of organic polymers (about 10 cm^2/V s) are competitive to amorphous silicon [13]

The demerits of organic semiconducting materials are

1. Band gap of the organic materials is large. Majority of semi-conducting polymer have band gap higher than 2 eV (620 nm). So, only a small portion of the incident solar light is absorbed [14].

2. In organic materials photoexcitation produces coulombically bound electron–hole pairs, called excitons. It is estimated that only 10% of the photoexcitations lead to free charge carriers in conjugated polymer [15].
3. Exciton diffusion length is very small about 10 nm.
4. Carrier mobilities of organic materials are low compare to single crystal Si.

CNTs are promising materials that act as exciton dissociating centers and ballistically conductive agent with high carrier mobility. In addition they are strong, rigid, chemically inert and environmentally resistant. CNTs are the cylindrical roll up graphene sheet whose length is in the micro scale and diameter in nano scale. Thus, it signifies large aspect ratios ($>10^3$). CNTs are classified by the number of rolled up graphene sheets. SWCNTs have only one rolled up graphene sheet in cylindrical structure. Nanotubes with many rolled up graphene layers are called multiwalled carbon nanotubes (MWCNTs). There is also a special class of MWCNTs called double walled carbon nanotubes (DWCNTs) which have two graphene layers rolled up with concentric center, that have different properties to SWCNTs and MWCNTs. Band gap of SWCNTs is inversely proportional to the tube diameter. By combining CNTs of different diameters and chiralities, correspondingly, different band gaps, it is possible to obtain a continuous response over a spectral range [16].

In 1999, a thin film of functionalized MWCNTs (f-MWCNTs) was used to make PV device using poly (p-phenylene vinylene) (PPV) [17]. Under illumination, the device (Al/PPV-MWCNTs/ITO) produced an open circuit voltage (V_{oc}), short circuit current (J_{sc}), fill factor (FF) and efficiency (η) were 0.9 V, 0.56 mA/cm^2, 0.23 and 0.081% respectively. The external quantum efficiency (EQE) of the device was twice than that of the ITO/PPV/Al devices. From observed EQE, it was estimated that holes are

accepted by f-MWCNTs at the PPV- functionalized MWCNTs interface. Later in 2002, it was also reported that SWCNTs transfer electron in the active layer of P3OT-SWCNTs composite [18]. In this device, arc generated SWCNTs were mixed with P3OT polymer. Diodes (Al/polymer-SWCNTs/ITO) show increase in the short circuit current by two order of magnitude compare to pristine polymer diode (Al/P3OT/ITO). It was proposed that the main reason for this increment is the photoinduced electron transfer at polymer/nanotube interface. After these major breakthroughs, most of the devices that are reported either claim in the increase of efficiency by incorporation of MWCNTs (enhancing hole conductivity) or SWCNTs (enhancing electron conductivity).

3.3 Polymer solar cell

Polymer solar cells are a type of flexible solar cell. It produces electricity from sunlight using polymers (or organic materials). This is because organic materials having delocalized π electron system can absorb sunlight, create photogenerated charge carriers and transport these charge carriers towards the electrodes.

3.3.1 Device Fabrication

The general device design for organic-CNTs solar cell is sandwich structure (Fig. 1) consisting transparent conducting electrodes (TCE) basically indium tin oxide (ITO) (marked with 'a' in Fig. 1), or fluorine tin oxide (FTO) coated on glass or polyethylene terephthalate (PET) substrate, poly (3,4-ethylenedioxythiophene) poly(styrenesulfonate) (PEDOT:PSS) (marked with 'b' in Fig. 1), active layer (CNTs–polymer) (marked with 'c' in Fig. 1) and a thermally evaporated metal electrode on the top of the composite layer typically aluminium 'Al' (marked with Al 'd' in Fig. 1)

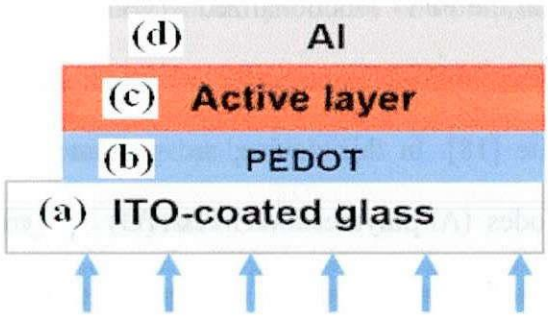

Figure 1 Common device structure for organic-CNTs solar cell.

Somewhere, 'Al' is also used with an ultrathin lithium fluoride (LiF) underlayer. Layer of PEDOT:PSS and LiF are generally called buffer layer. Ultrasonication method is used to disperse CNTs in the conjugated polymer, followed by centrifugation to remove large aggregates. The composite solution is then deposited on the transparent electrode either by drop casting or spin coating.

3.3.2 Charge Separation

In organic materials, photon absorption generates bound electron–hole pairs, so called "excitons". These excitons have to dissociate into free charges in order to get photovoltaic response. Figure 2 shows schematic energy-band diagram of a simple device consisting of a single organic layer between two electrodes of different work functions, i.e. Au and ITO. The difference in the work function of these electrodes generates electric field, which is sufficient to break up the photogenerated exciton. Since, exciton diffusion length is short, (about 1–10 nm) in single layer and the mobility is low, there are a lot of chances of recombination or break up to supply separate charges. Thus, quantum efficiency (QE) of this type of solar cell is less than 1%.

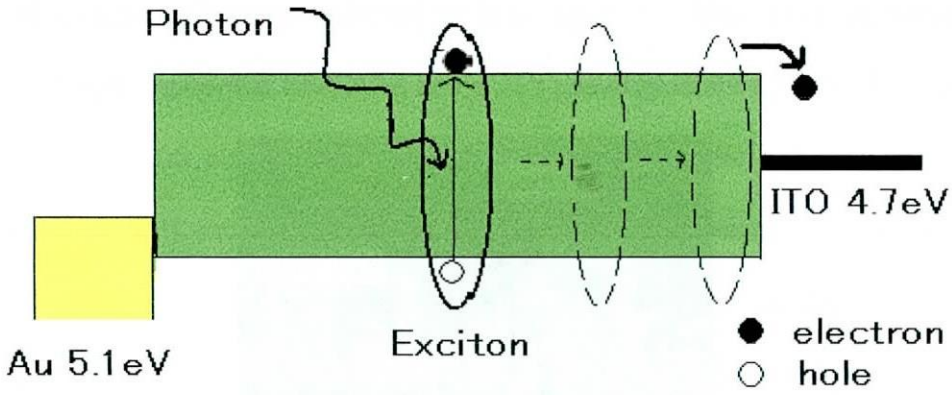

Figure 2 Schematic energy-band diagram of a simple device consisting of single organic layer between two metal contacts. An electric field results from the difference in work functions of the contacts. Absorbed photons generate excitons that diffuse towards one or other contact (here it is diffusing towards ITO contact) where they may dissociate to yield charge pairs.

In bulk heterojunction, materials of higher electron affinity (like C_{60}, PCBM, CNTs) can dissociate excitons. This allows the preferential transfer of the electrons into electron acceptor molecule (like C_{60}, PCBM, SWCNTs), while leaving holes to be transported through the polymer. This process of charge separation is known as photoinduced charge transfer. But in heterojunction (suppose P3HT-C_{60}), electrostatic forces result from the differences in electron affinity and ionization potential. If both electron affinity and ionization potential are greater in one material (the electron acceptor, say C_{60}) than the other (the electron donor, say P3HT) then the interfacial electric field drives charge separation [19]. The local electric field is strong and may break up photogenerated excitons. However, the better understanding of the charge separation in polymer–CNTs interface is still in progress. The large band gap of organic materials to small band gap semi-conducting CNTs may generate 'build in voltage'. The

high electric field (or build in voltage) in these junctions can split up the excitons. The photoinduced charge transfer between P3OT and SWCNTs is shown in Fig. 3.

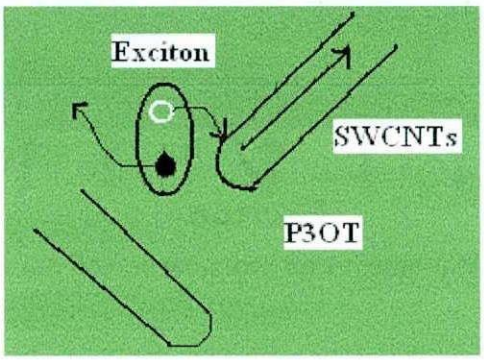

Figure 3 Dissociation process of photogenerated exciton on polymer-SWCNTs blend. Electron is transferred to SWCNTs

Layer assembly is a way of using CNTs films at different layers of device. Chaudhary et al. [20] studied the effect of thin layer of SWCNTs by placing it at different layers in the device. They noted that SWCNTs on the hole collecting side of the active layer leads to an increase in the power conversion efficiency (PCE) of the PV devices from 4 to 4.9%. The success of the device performance depends on appropriate purification processes [21–24], chemical functionalization [24–28], individualization [29, 30], length shortening [30] and crystallinity [31, 32]. CNTs films are generally produced after functionalization. This is because f-CNTs get dissolved in polar and non polar solvent.

3.3.3 Functionalization of CNTs

Non-functionalized CNTs are insolubility. A number of methods have been reported to functionalize CNTs [23–27]. Edge sites of CNTs are much more reactive than the atoms in the interior of the graphene cylinder and chemisorbed foreign elements. Surface oxides are produced by liquid oxidants e.g. aqueous solutions of H_2O_2, NaOCl, $(NH_4)_2S_2O_8$, $AgNO_3$, H_2PtCl_6 etc. The surface oxides decompose to CO_2 or CO on

heating. After cooling to room temperature, they may again react with oxygen (air) or water vapor. It is shown that SWCNTs whose lengths have been reduced by sonication (in range of 100–300 nm) can be soluble in common organic solvents by covalent functionalization [29]. Functionalization of CNTs starts from simple ultrasonication [33, 34] to complex chemical treatment. Titration, infrared spectroscopy (IR), X-ray photoelectron spectroscopy, thermal desorption spectroscopy, electrokinetic measurement are the most frequently used methods for the characterization of surface oxides [35]. Oxidation with HNO_3 is considered as mild oxidation method and often used because its oxidizing properties can be controlled by concentration and temperature. It is suggested that HNO_3 introduces carboxylic acid groups (COOH) only at those initial defects that already exist (like edges of CNTs). In contrast, sonication of CNTs in mixture of H_2SO_4 and HNO_3 increases the incidence of carboxylic acid groups not only at initial defect sites but also created new defect sites along the walls of CNTs. The oxidation processes begin at initial defects at first and followed throughout the CNTs length. Strong oxidation like cutting of CNTs [29] begins from newly developed defect sites in CNTs, can be divided into two steps: (1) the defect-generating step and (2) the defect consuming step. During defect generating step, the oxidants attack the graphene structure by electrophilic reactions and generate active sites like OH, C=O. During defect consuming step, the graphene structure of the tube was destroyed [24]. For chemistry of CNTs see reference [36-43]. Once oxidized, the nanotubes spontaneously dispersed in water and remain stable for many months with only a very small amount of aggregation materials precipitation over time. Precipitation could be accelerated by ionic additions, particularly acidic ones. The oxidation of nanotubes induces a negatively charged surface, particularly through the ionization of acidic surface groups [37, 38]. The resulting electrostatic repulsion leads to a dramatic increase

in the stability of the colloidal dispersion. Zhang et al. [38] suggest that $KMnO_4$ and dilute HNO_3 are all inefficient in the defect-consuming step whereas the acid mixture (H_2SO_4/HNO_3) is strong enough to cut the graphite structure and generated carboxylic group with increasing treatment time. Carboxylic group helps to dissolve CNTs in solvent that makes possible of preparing CNTs films by spin coating or drop casting. T. V. Sreekumar et al. [43] observed conductivity in the plain of functionalize CNTs film is $1x10^5$ S/m. This film reduces conductivity after annealing. However, in microwave functionalized SWCNTs film, conductivity was regain after annealing in inert atmosphere [44].

3.3.4 Chemical treatment on energy level of CNT films

H. Ago et al. [45] studied the change in the DOS of acid treated MWCNTs. They showed that oxidized MWCNTs affect work functions. The calculated work function of MWCNTs using ultraviolet photoelectron spectroscopy (UPS) are listed in Table 1.

Table 1.Work Function of MWCNTs and Graphite determined from UPS [Source 45]

Sample	Work function(eV)
Purified MWCNTs	4.3
air-oxidized MWCNTs	4.4
plasma-oxidized MWCNTs	4.8
acid-oxidized MWCNTs	5.1
Highly oriented pyrolytic graphite (HOPG)	4.4

UPS is a powerful technique for the investigation of both the valence band DOS and the work function. Authors have proposed the following reasons for changing the work functions

(i) The lower work function of MWCNTs to HOPG is due to destabilization of the π- electron due to the curvature of the graphene sheets.

(ii) The higher work function of functionalized MWCNTs is due to the reduction of the π conjugation of the MWCNTs, which reduces the pπ derived DOS. Such reduction is due to the transformation of the graphene layers to amorphous carbon phase with sp^3 networks and due to the enhancement of surface dipoles because of oxygen-containing functional groups.

3.4.5 Improvement of polymer solar cell by CNTs incorporation

The advantages of CNT incorporation in polymer solar cell are summarized as follows:

1. In SWCNTs-epoxy composites, the electrical conductivity has been claimed to rise by nearly 10^5S/cm between 0.1 and 0.2% weight loading of SWCNTs [30]. Hence, CNTs improve low carrier mobilities of organic material.
2. CNTs provide high surface area (~1,600 m^2/g), which offers a tremendous opportunity for exciton dissociation.
3. Since SWCNTs have diameters in nanoscale and lengths on the order of microns, so at low doping of SWCNTs, percoration pathway are established providing the means for a high carrier mobility and efficient charge transfer. However, such pathways are not established in polymer solar cell. Recently, there are some reports of fabrication of polymer nanofibers for creating pathway in enhance hole mobility. Thus, CNTs provide large interfacial area for low exciton diffusion length of polymer.

4. CNTs have low energy gap compared to large energy gap of organic polymer. The lower band gap of CNTs and higher band gap of polymer materials may generate a large build in voltage. Charges may separate at this built in field.
5. CNTs make percolation pathway for charge transformation. However, in polymer–C_{60} composition, electrons transfer by hopping.

Other beneficial properties of SWCNTs relevant to polymeric photovoltaic development include composite reinforcement and thermal management. Tensile strengths of SWCNTs have been estimated to equal ~20 GPa, while the Young's modulus measured by atomic force microscopy is ~1 TPa. This high Young's modulus and strength to weight ratio could provide much needed mechanical stability to large area thin film arrays [46].

3.4 Fabrication and properties of organic/CNTs-Si heterjunction solar cell

Since the discovery of photoinduced charge transfer between organic conjugated polymer and nanotubes, both MWCNTs and SWCNTs have been used to fabricate photovoltaic devices. Functionalized MWCNTs [47], functionalized SWCNTs [48], C_{60}-decorated SWCNTs [49], C_{60}-decorated MWCNT [50] have shown better power conversion efficiency than pristine samples without CNTs. In such solar cells, it is suggested that MWCNTs enhance hole transport, whereas SWCNTs enhance electron transport. On the other hand, functional groups of CNTs make homogeneous blend of CNTs-polymer composite. This may be because CNTs are soluble in organic solution after functionalization. Furthermore, CNTs films have been extensively used for making photovoltaic devices. CNTs films can be fabricated at low cost by drop casting, spin coating, Langmuir–Blodgett deposition, etc. Ago et al. [45] obtained photovoltaic

response of conjugated polymer in thin film of f-MWCNTs under the visible light. Recently, high transparency, tunable work function metal wire grid electrodes have been reported for the application in organic solar cell. The fabrication of organic photovoltaic devices on flexible ITO coated plastic [polyethylene terephthalate (PET)] substrate, transfer-printing method, and role-to-role-type manufacturing makes them to be integrated into existing building structures, which is impossible by conventional technologies. Detail description is given in ref [51].

3.4.1 Experimental details

A large quantity of CNTs was synthesized on supporting materials and then purified. Purified MWCNTs were suspended in 50 ml of a 3:1 mixture of concentrated H_2SO_4/HNO_3 and sonicated in a water bath for a few hours. The resultant suspension was then diluted with de-ionized water and MWCNTs were collected on pore membrane filter. SWCNTs (0.1 mg) and f-MWCNTs (0.1 mg) were dispersed together in 1 ml of chloroform solvent. A known quantity of P3OT (6 mg/mol) was dispersed separately in another chloroform solvent. Prepared solutions of CNTs were spin coated at 600 rpm over n-Si substrates. Microscopically porous CNT film is then infiltrated with P3OT polymer solution. Care is taken to make a thin film of P3OT over CNT networks. Fabricated films were annealed at 120°C for 15 min. In doing so, mesoscopic order and crystallinity of organic polymer materials increase. From the viewpoint of the relationship between structure and performance, a nanocrystalline structure with high crystallinity is pursued so that a relatively high transportation speed for holes is obtained via interchain transport of charge carriers. Finally, semitransparent gold electrodes (20–30 nm) were deposited by sputtering.

3.4.2 Characterization

The infrared absorbance was recorded using a Perkin Elmer Fourier transform infrared (FTIR) spectrometer. An atomic force microscopy (AFM) image was obtained by Spa 300 SII Seiko Instrument. Gold electrodes were deposited by sputtering of gold target in E-1030 ion sputter. Current-voltage (I-V) characteristics were measured at room temperature using JASCO SS-200 W solar simulator in the dark and under AM 1.5 simulated solar radiation.

3.4.3 Result and discussion

Figure 1 shows a FTIR spectrum of the f-MWCNTs. After acid treatment, the tubes are not only cut into short pipes but also purified because of intercalation and exfoliation of graphite. This method is more effective than gas-phase oxidation method because CNTs are believed to be functionalized throughout the tube length. Peak at around 1730cm−1 is assigned to the C = O strength vibration in the COOH group. It has been realized that acid-oxidized MWCNTs are dispersed in polar and nonpolar solvent, which in turn can be very useful for further processing. X-ray photoelectron spectroscopy measurement of acid-oxidized MWCNTs shows formation of carboxylic group[45].

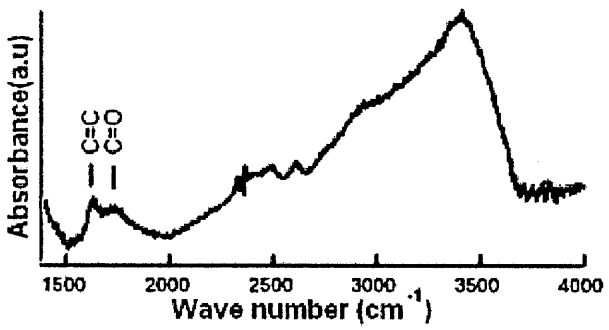

Figure 4. FTIR spectrum of MWCNTs obtained after acid treatment

Figure 5a shows the schematic of the P3OT/n-Si (organic-inorganic heterojunction) solar cell incorporating CNTs (f-MWCNTs and SWCNT). Figure 5b shows the I-V characteristics in dark and under AM 1.5 simulated solar radiation for n-Si/f-MWCNTs+SWCNTs-P3OT heterojunction solar cell with partially transparent gold upper electrode (20–30 nm). Direct contact was made to the silicon by conducting stainless steel stage, and the cell was illuminated from gold electrode side. Under illumination, short circuit current density (Jsc) and open circuit voltage (Voc) are about 6.16mA/cm2 and 0.44 V, respectively. The fill factor (FF) and white light conversion efficiency (η) are about 0.36 and 0.98% respectively. Table 2 lists photovoltaic properties of solar cells fabricated by similar conditions using various kinds of composites. It is obvious that f-MWCNTs+SWCNTs-P3OT composite showed better power conversion efficiency among these samples [50,53-57] A twin reference cell fabricated in the same manner with only P3OT film (without CNTs) with identical device parameters shows no good photovoltaic effect. This may be due to the fact that exciton dissociation would occur only at P3OT/n-Si interface and hole transport across P3OT layer is restricted due to the low mobility, whereas in n-Si/f-MWCNTs+SWCNTs-P3OT device, CNTs make a network throughout the composite layer and provide direct pathway to enhance carrier transfer.

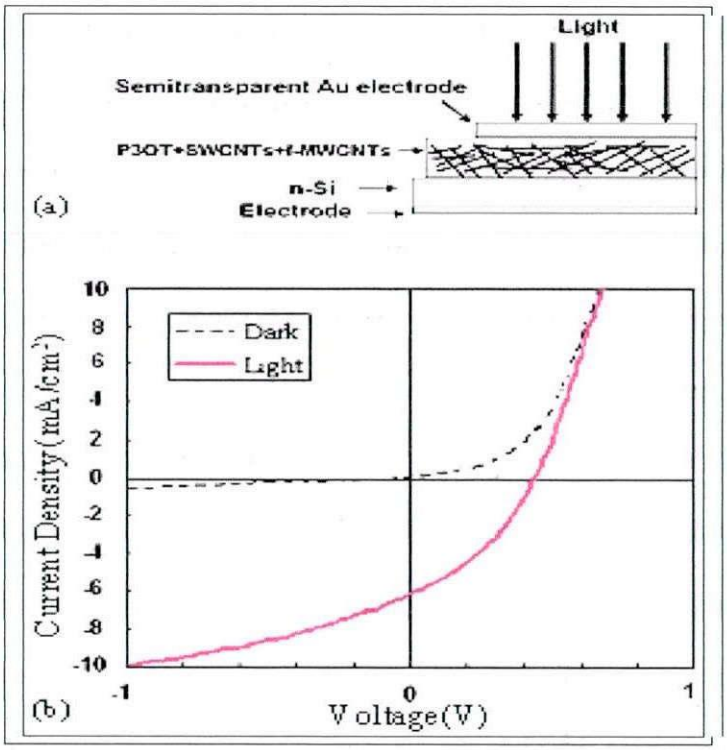

Figure 5 (a)Schematic of the P3OT/n-Si heterojunction solar cell incorporating f-MWCNTs and SWCNTs in the polymeric layer (b) Current voltage(I-V) characteristics of the n-Si/f-MWCNTs+SWCNTs+P3OT/Au heterojunction solar cell in the dark and under AM 1.5 simulated solar radiation. Cell is illuminated from the semitransparent Au electrode side.

With the introduction of f-MWCNTs and SWCNTs in the photoactive layer, there is large improvement in power conversion efficiency. It is believed that such enhancement in power conversion is due to the efficient electron transportation through SWCNTs and efficient hole transportation through f-MWCNTs. The work function of SWCNTs ranges from 3.4 to 4 eV, while for MWCNTs the range is from 4.6 to 5.1 eV. Acid oxidation introduces carboxylic acid groups on the surface of MWCNTs and produced higher work function (5. 1eV). In our f-MWCNTs, the carboxylic acid group was

examined. It suggests that work functions of SWCNTs and f-MWCNTs are closer to the conduction band and valance band of P3OT, which signifies possible electron and hole transportation, respectively. Increased work function of f-MWCNTs brings MWCNTs in same level of Au (5.1eV), which enhances hole transportation toward anode. Energetically favorable charge transportation and band diagram is shown in Fig. 6.

Table 2. Photovoltaic characteristics of solar cells under AM 1.5 simulated solar radiation obtained from different composition [51].

No.	Composites	Jsc(mA/cm2)	Voc(V)	FF	η(%)	Ref.
i	C_{60}-O-MWCNTs/P3OT	1.68	0.245	0.27	0.11	[50]
ii	DWCNTs/P3HT	0.3398	0.446	0.17	0.026	[53]
iii	MWCNTs/P3OT	2.915	0.22	0.27	0.175	[54]
iv	C_{60} nanorod/P3OT	0.0098	0.155	0.1485	0.0002	[55]
v	Pt-MWCNTs/P3OT	5.88	0.3396	0.3876	0.775	[56]
vi	Cut-MWCNTs/P3OT	7.65	0.23	0.31	0.54	[57]

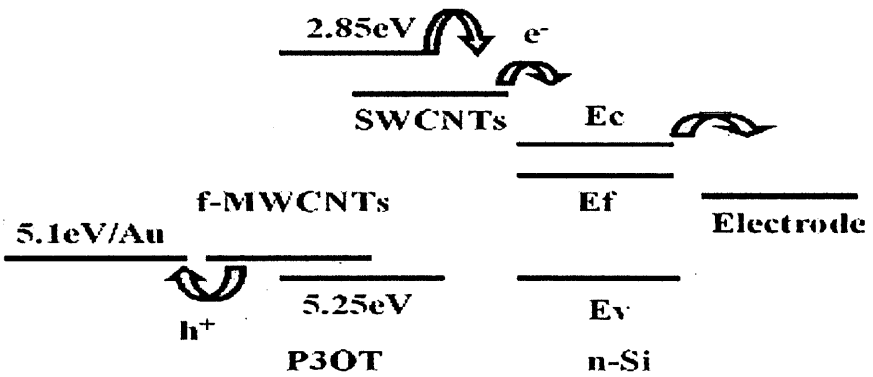

Figure 6 Energy band diagram of the fabricated device showing band alignment for f-MWCNTs and SWCNTs.

In the photovoltaic device with SWCNTs and f-MWCNTs, P3OT acts as the photoexcited electron donors and SWCNTs act as electron acceptor and provide percolation paths. The mobility of MWCNTs is several orders higher in magnitude compared to that in the polymer, which may result in the enhancement of hole transport. In addition, CNTs may serve as "conducting bridges" connecting the polymer chains.

3.5 Conclusion

In summary, organic-inorganic heterojunction solar cells were fabricated by incorporating both SWCNTs and f-MWCNTs. FTIR measurement conformed oxygen containing functional group in MWCNTs. SWCNTs and f-MWCNTs were mixed together and dispersed in chloroform solvent. For solar cell fabrication, P3OT was infiltrated in microscopically porous CNTs film. By introducing f-MWCNTs and SWCNTs together, an improvement in the photovoltaic response was observed. The reason for such increment might have come from tunable work function of CNTs. It is believe that the work function of SWCNTs and f-MWCNTs are closer to the conduction band and valance band of P3OT, which signifies possible electron and hole transportation, respectively.

References

1. Nanostructured Materials for Solar Energy Conversion, T.Soga, Chapter1. Elsevier (2006)
2. J. Robertson, Mater. Sci. Eng.R 37 (2002)129
3. A.K.Geim, K.S. Novoselov, Nat. Mater. 6, (2007) 183
4. H.W. Kroto, J.R. Health, S.C.O'Brien, R.F. Curl, R.E.Smalley, Nature 318 (1985) 162
5. S.Iijima Nature 354, (1991) 56
6. X.Wang, L.Zhi, N. Tsao, Z.Tomovic, J. Li, K. Mullen,. Angew. Chem. Int. Ed., 47 (2008) 2990
7. W.Ma, L.Song, R.Yang, T. Zhang, Y. Zhao, L. Sun, Y. Ren, D.Liu, L. Liu, J. Shen, Z. Zhang, Y. Xiang, W. Zhou, Z. Xie, Nano Lett. 7 (2007) 2307.
8. H. Peng, J. Am. Chem. Soc. 130 (2008) 42.
9. H.Koezuka, A.Tsumara, T.Ando, Synth. Met. 18 (1987) 699.
10. H.Hoppe, N.S.Sariciftci, D. Meissner. Mol. Cryst. Liq. Cryst., 385 (2002) 113.
11. J, Roncali, Chem. Rev. 97 (1997) 173.
12. J.Zou, L.Liu, H.Chen, S.I.Khondaker, R.D.McCullough, Q.Huo, L.Zhai, Adv. Mater.20 (2008) 2055.
13. C.D. Dimitrakopoulos, P.R.L. Malenfant Adv. Mater 14 (2002) 99.
14. J.M.C.R. Nunzi Physique, 3 (2002) 523.
15. E.Kymakis , G.A.J. Amaratunga, Appl. Phys. Lett. 80 (2002) 112.
16. S. Kazaoui, N.Minami, B.Nalini, Y.Kim, K.Hara, J. Appl. Phys. 98 (2005) 084314.
17. H.Ago, K. Petritsch, M.S.P. Shaffer, A.H. Windle, R.H. Friend, Adv. Mater. 11(1999), 1281.
18. P. B.Miranda, D. Moses, A.J. Heeger, Phys. Rev. B 64 (2001) 81201.

19. J.J.M. Halls, K.Pichler, R.H. Friend, S.C. Moratti, A.B.Holmes, Appl. Phys. Lett. 68,(1996), 3120.

20. S.Chaudhary, H.Lu, A. M. Muller, C.J. Bardeen, M. Ozkan, Nano Lett.,7(2007) 1973.

21. A. R. Harutyunyan, B. K. Pradhan, J. Chang, G. Chen, P. C. Eklund: J. Phys. Chem. B. 106 (2002) 8671.

22. K. Tohji, H. Takahashi, Y. Shinoda, N. Shimizu, B. Jeyadevan, I. Matsuoka, Y. Saito, A. Kasuya, S. Ito, Y. Nishina, J. Phys. Chem. B 101(1997) 1974.

23. Y. Lian, Y. Maeda, T. Wakahara, T. Akasaka, S. Kazaoui, N. Minami, T. Shimizu, N. Choi, H. Tokumoto, J. Phys. Chem. B 108 (2004) 8848.

24. J. Zhang, H. Zou, Q. Qing, Y. Yang, Q. Li, Z. Liu, X. Guo, Z. Du, J. Phys. Chem. B 107 (2003) 3712.

25. J. Liu, M. Rodriguez, I. Zubiri, M. Dossot, B. Vigolo, R.H. Hauge, M. Dossot, Y. Fort, J. J. Ehrhardt and E. McRae, Carbon 45 (2007) 885.

26. J. Chen, M. A. Hamon, H. Hu, Y. S. Chen, A. M. Rao, P. C. Eklund, R. C. Haddon: Science 282 (1998) 95.

27. Y. Qin, J. Shi, W. Wu, X. Li, Z.X. Guo, D. Zhu, J. Phys. Chem. B 107 (2003) 12899.

28. N. I. Kovtyukhova, T. E. Mallouk, L. Pan, E. C. Dickey, J. Am. Chem. Soc., 125 (2003) 9761.

29. J. Liu,A. G. Rinzler,H. Dai,J. H. Hafner,R. K. Bradley,P. J. Boul,A. Lu,T. Iverson,K.Shelimov,C. B. Huffman,F. R-Macias,Y.-S. Shon,T. R. Lee,D. T. Colbert,R. E. Smalley, Science, 280 (1998) 1253.

30. A. Pénicaud, P. Poulin, A. Derré, E. Anglaret, P. Petit, J. Am. Chem. Soc. 127 (2005) 8.

31. V. Georgakilas, K. Kordatos, M. Prato, D.M. Guldi, M. Holzinger, A. Hirsch, J. Am. Chem. Soc., 124 (2002) 760.

32. W. Zhao, C. Song, P.E. Pehrsson, J. Am. Chem. Soc. 124 (2002) 12418.

33. A. Koshio, M. Yudasaka, M. Zhang, S. Iijima, Nano Lett. 1 (2001) 361.

34. S. Niyogi, M. A. Hamon, D. E. Perea, C. B. Kang, B. Zhao, S. K. Pal, A. E. Wyant, M. E. Itkis, and R. C. Haddon, J. Phys. Chem. B,107 (2003) 8799.

35. H.P. Boehm, Carbon 40 (2002) 145.

36. S. Niyogi, M.A. Hamon, H. Hu, B. Zhao, P. Bhowmick, R. Sen,. M.E. Itkis, R.C. Haddon, Acc. Chem. Res. 35 (2002) 1105.

37. K. Esumi, A. Ishigami, A. Nakajima, K. Sawada, H. Honda, Carbon , 34 (1996) 279.

38. M.S.P. Shaffer,X.Fan, A.H. Wandle,. Carbon 36 (1998) 1603.

39. I. Khatri, N. Kishi, J. Zhang, T. Soga, T. Jimbo, S. Adhikari, H.R Aryal, M. Umeno, Thin solid films 518 (2010) 6756.

40. D.S. Knight, W.B. White, J. Mater. Res. 4 (1989) 385.

41. J. Kastner, T. Pichler, H. Kuzmany, S. Curran, W. Blau, D.N. Weldon, M. Delamesiere, S. Draper, H. Zandbergen, Chem. Phys. Lett. 221(1994) 53.

42. T. W. Scharf and I. L. Singer Third Bodies and Tribochemistryof DLC Coatings 2007, SpringerLink.

43. T. V. Sreekumar, T. Liu, S. Kumar, L. M. Ericson, R. H. Hauge, R. E. Smalley, Chem. Mater. 15 (2003) 175.

44. Y.Wang, Z. Iqbal, S.Mitra, J.Am.Chem.Soc. 128 (2006) 95.

45. H. Ago, T. Kugler, F. Cacialli, W. R. Salaneck, M. S. P. Shaffer, A. H. Windle, and R. H. Friend, J. Phys. Chem. B 103 (1999) 8116.

46. I. Khatri, T. Soga. Chapter 5, Oxide and Nanomaterials (2011) 101

47. C. Li, S.Mitra,. Appl.Phys.Lett.91 (2007) 253112.

48. A. J. Miller, R. A. Hatton, S. R. P. Salva, Appl. Phys. Lett. 89 (2006) 123115.

49. C.Li, Y. Chen, Y. Wang, Z.Iqbal, M.Chhowalla, S.Mitra J.Mater.Chem. 17 (2007) 2406.

50.G..Kalita, S.Adhikari, H.R.Aryal,M.Umeno, R.Afre, T.Soga, M.Sharon, Appl.Phys.Lett. 92 (2008) 063508.

51. I.Khatri, S.Adhikari, H.R.Aryal, T.Soga, T.Jimbo, M.Umeno, App.Phys.Lett.94 (2009) 093509.

52. I.Khatri,T.Soga,T.Jimbo,S.Adhikari,H.R.Aryal,M.Umeno,DiamondRelat.Mater.,18 (2009) 319.

53. S.P. Somani ,P.R.Somani,M.Umeno, E.Flahaut, Appl.Phys.Lett. 89 (2006) 223505.

54. S.P. Somani,P.R.Somani, M.Umeno,. Diamond Relat.Mater.,17(2008)585.

55. P.R. Somani ,S.P.Somani,M.Umeno, Appl.Phys.Lett. 91 (2007) 173503.

56. P.R. Somani ,S.P.Somani, M.Umeno, Appl. Phys. Lett.93 (2008) 033315.

57.G.Kalita,S.Adhikari,H.R.Aryal,M.Umeno,R.Afre,T.Soga,M.Sharon,Appl.Phys.Lett. (2008) 123508.

CHAPTER 4

LAMINATED SOLID STATE DYE SENSITIZED SOLAR CELL

CHAPTER 4
LAMINATED SOLID STATE DYE SENSITIZED SOLAR CELL

Organic photovoltaic (OPV), provides promise of a low cost solar photovoltaic solution and attracts significant academic and industry research. Organic semiconducting materials having delocalized pi (π) electron system can absorb sunlight, create exciton and transport photogenerated charge carriers. They have higher absorption coefficients, therefore active layer of a few hundreds of nanometer range are enough. Electronic band gap of the materials can be controlled by chemical synthesis. Polymer-fullerene bulk heterojunction PV fabricated from blends have been extensively studied showing several breakthroughs in efficiency [1, 2, 3]. Every year new record on power conversion efficiency (PCE) of organic solar cell is being set. Mitsubishi Chemical reportedly set a new efficiency record, producing organic solar cells with 9.2% conversion efficiency. Meanwhile, Konarka Technologies, Solarmer Energy Inc., and Heliatek—are now reporting cells with efficiencies greater than 8% [4]. These results pave towards commercialization of the techniques. It is predicted that OPVs devices achieve 10% efficiency from single layer device and around 15% in tandem structure [5]. However, the conventional device architecture which consists of a poly(3,4-ethylenedioxythiophene) :poly(styrenesulfonate) (PEDOT :PSS) as hole-collecting layer and a bulk-heterojunction layer (polymer-fullerenes), sandwiched between ITO or FTO and a low work function metal electrode are consider not efficient for higher power conversion efficiency and long stability. The low work function metal electrode in this device geometry can be easily oxidized in air leading to deterioration in performance. To address this problem, a new device architecture using a titanium oxide (TiO_x) or zinc oxide (ZnO) buffer layer between the organic active layer and ITO substrate has been introduced as a hole blocking and oxygen barrier layer to improve the device stability. Therefore, the concept of inverted device architecture was introduced [6-9]. The name 'inverted' describes the reversed change in polarity of solar cell. For

example, in ITO/PEDOT: PSS/P3HT: PCBM/Al device structure, ITO and Al electrodes collect hole and electron respectively. But in inverted device structure, proper n or p-type interfacial layers or both (n-type and p-type) interfacial layers are introduced either on ITO or metal electrode or both, which change the polarity of the solar cell. Therefore, the name 'inverted' is given to these type of solar cell. In inverted architecture, the polarity of charge collection is opposite to the conventional architecture allowing the use of higher work functions metals (Au, Ag, Cu) as top electrodes. These electrodes are air-stable and make good contact with organic layers. The use of higher work function metals offer better ambient interface device stability and the possibility of using non-vacuum coating techniques to deposit the top electrode helping to reduce fabrication complexity and costs [10-13]. High-energy band gap materials such as zinc oxide (ZnO) [14,15], titanium oxide (TiO_x) [16-18], cesium carbonates (Cs_2CO_3) [19,20], calcium (Ca) [21] are coated on ITO substrates for efficient electron transportation whereas, hole collecting layers like molybdenum trioxide (VI) (MnO_3) [22-26], vanadium oxide (V_2O_5) [27-28], tungsten oxide (WO_3) [30,31] and solution processed conducting polymer poly(3,4-ethylenedioxythiophene) poly(styrenesulfonate) (PEDOT:PSS) [32-34], sulfonated poly(diphenylamine) (SPDPA) [35] at the top of active organic layer before deposition of higher work function metal electrodes. Such interfacial layers play important roles (a) to suppress contact resistance between the organic and charge collecting electrodes [14-35] (b) change non-Ohmic contact to Ohmic contact [19] (c) efficient charge transportation [14-36].

Furthermore, based on the light source illuminating, the inverted architecture is differentiated into top illuminated or bottom illuminated inverted solar cell. The top illuminated architecture utilizes a reflective buried bottom electrode and a semi-transparent top electrode whereas the bottom illuminated inverted architecture

configuration utilizes a higher work function reflective electrode as the top hole collecting contact and semi-transparent conducting electrode (like ITO, FTO) at the bottom to collect electrons. In top illuminated inverted solar cell, it is important to note that the bottom electrode is metal foil instead of a glass substrate. Ag, ITO, Cs_2CO_3, Al is generally deposited in the metal foil for the reflection of visible light. The detailed review on inverted polymer solar has been given elsewhere [37].

4.1 Laminated polymer solar cell

Inverted polymer solar cell architecture is an efficient way to improve the efficiency of OPVs. It can be further simplified by stamping or laminating top metal electrodes for roll-to-roll fabrication [38-41]. Direct vacuum evaporation of the metal electrodes on the active polymeric layer could damage the surface morphology of the device reducing device performance [42-47]. To overcome these problems, stacking [38-41] or stamping [48- 52] the two active layers of the device in BHJ solar cell was introduced. Stacking or stamping as a method of device fabrication has several advantages over conventional bottom up device fabrication process. (a) The power conversion efficiency (PCE) of the stacking (or laminated) device is almost similar or higher to the devices fabricated from the evaporated top metal electrode [38-41]. (b) Laminated interface produces ohmic contact to another layer showing high fill factor and low series resistance [40]. (c) The processing step of thermal evaporation of a metal onto the active layer is eliminated which reduces the high parasitic resistance that may create from conventional metal evaporation [38, 39]. (d) It enables the in-air fabrication of devices [38-41]. (e) It produces a self-encapsulated device that is mechanically protected on both sides [40]. (f) The methodology allows one to prepare, optimize and characterize two parts of the device independently before bringing them to contact [38-41]. (g) All solution processing fabrication of device is possible. (h) It is cost

effective and simple method. (i) It allows the fabrication of multilayer photovoltaic devices [38].

One way to fabricate multijunction solar cell is by connecting two polymer blend layers with introduction of a (semi) transparent metal or semiconducting layer between the blend layers, which is generally named as tandem solar cell. In tandem structure, the intermediate layer works as charge recombination center; therefore the device has an open circuit voltage (V_{oc}) that is the sum of the values of two devices, whereas short circuit (I_{sc}) of the device is restricted to the smaller value of the two. On the other hand, a "multilayer device" in which the two active layers are stacked directly (i.e without any interfacial layer) has an J_{sc} value that is the sum of the values for the two cells. Recently, Sun et al. [53] demonstrated the fabrication of multilayer structure solar cell from solution-processing method. This unique temperature dependent solubility of poly(2,5-bis(3-alkylthiophen-2-yl)thieno[3,2-b]thiophene) (PBTTT) enabled them to spin-coat a solution of PBTTT at 70 °C and another overlaid polymer (MDMO-PPV) from the same solvent at room temperature without dissolving the underlying PBTTT layer. As a result, the fabrication of multilayer BHJ solar cells from all-solution process was achieved. Postannealed bilayer bulk-heterojunction devices yielded a V_{oc} of 0.59V, J_{sc} values of 10.1-10.7mA/cm^2, FF of 0.55, and PCE of 3.0-3.2%, showing an increased J_{sc} and PCE by a factor of 2 with respect to their single layer counterparts. Preparation of multilayer device from solution processing is a difficult task because the underlying polymer layer may dissolve from the solution processing of the second polymeric solution. The follow-up work by Nakamura et al. demonstrates the fabrication of multilayer structure BHJ solar cell from lamination process [38,54]. Multilayer structures consisting of two blend layers of poly(3-hexylthiophene) (P3HT):(6,6)-phenyl C61 butyric acid methyl ester (PCBM) and

poly{N-[1-(2′-ethylhexyl)-3-ethylheptanyl]-dithieno[3,2-b:2′,3′-d]pyrrole-2,6-diyl-alt-4, 7-di(2-thienyl)- 2,1,3-benzothiadiazole-5′,5″-diyl} (PDTPDTBT):PCBM were prepared by a simple thermal lamination technique under heat and pressure. The device structure is Glass/Au/PEDOT:PSS/ P3HT:PCBM // PDTPDTBT:PCBM / TiO_2 / ITO/Glass, whereas // represent interfacial layer. Now, throughout the chapter // represents an interfacial layer. They demonstrated improvement in PCE of inverted-structure laminated photovoltaic devices from 1.6% to 2.6% based on single structural BHJ solar cell [38]. The insertion of a PEDOT: PSS layer, between the metal electrode and polymer layer further improved the PCE to 3.3 %. A compact layer of TiO_2 is necessary on the cleaned ITO substrate to make hole blocking layer. However, lamination of two parts of the device to finish the final OPV structure was shown a decade ago for polymer-polymer bilayers [55].

Heat and pressure are important parameters to laminate two different electrodes. Nakamura et. al. suggested that adhesive materials was not necessary when heat and pressure were applied simultaneously[38,54.]. But B. A. Bailey et al. noticed that 25% of devices without adhesive material delaminated when plates of the press were pull apart, while none of the devices delaminated with adhesive material when plates of the pressure were pull apart [40]. In their work, they mixed conducting polymer (d-sorbitol) with PEDOT:PSS to improve adhesive property. D:sorbitol is a transparent glue, exhibiting a conductivity of $10^2 Scm^{-1}$ that could effectively laminate various substrates electrically and mechanically [41]. The conductivity of a PEDOT: PSS film could be enhanced by adding an organic compound with multiple polar groups or treating the PEDOT: PSS aqueous solution/film with an organic compound having multiple polar groups. The PEDOT:PSS (d-sorbitol) film is able to laminate two substrates well and free of solvent. D-sorbitol melts penetrates into the polymer at temperature above

98-100°C [41]. B.A. Bailey et al. selected flexible conducting substrate (PET) as anode to fabricate laminated solar cell with PET/Ag/PEDOT:PSS (d-sorbitol)// P3HT:PCBM/ZnO/ITO/glass configuration. The PET substrates improve device reproductively because of its flexible nature. Non-flexible glass substrate may break with pressure during lamination. The best-laminated device shows PCE of 3.19%, which is higher than the control devices produced with the best evaporated top metal electrode. Such improvement comes from the increased work function of Ag metal electrode with air oxidation [40]. Similarly, Y. Yuan et al.[39] increases the work function of Ag film by ultraviolet/ozone treatment for improved photovoltaic response. This treatment increases the coverage of the adhesive material (d-sorbitol) from 70% to 100%. The device architecture was PET/Ag/d-sorbitol//P3HT:PCBM/Cs_2Co_3/ITO/glass. Hot plate lamination also promotes the crystallization of PCBM material [39]. This method has been suggested for the roll-to-roll mass production of OPVs. Under the one sun simulated irradiation, the device with laminated PET/Ag/d-sorbitol anode shows the highest PCE compared to devices with laminated PET/ITO/d-sorbitol or PET/Al/d-sorbitol anode. The reduction of device performance in PET/ITO/d-sorbitol architecture is believed due to (a) the increase in sheet resistance of ITO substrates during multiple bending and (b) penetration of ITO fragments into the soft polymer layers during the lamination process that may form current leakage paths. Similarly, improvements in device performance with PEN/Ag/d-sorbitol anode has been explained as (a) better light harvest from the light reflection from top Ag anode film (b) Efficiently charge collection and (c) Oxidation of Ag surface increases the anode work function and surface energy.

4.2 Solid state dye sensitized solar cell using conjugated polymers as hole transport materials.

Materials and technique that are required to fabricate inverted and laminated OPVs are almost same and similar to the materials and technique required to fabricate solid state dye sensitized solar cell (s-DSSCs) that use conjugated polymers as HTMs. In inverted organic solar cell, ZnO, TiO_x layer are in nanometer thickness whereas in s-DSSCs with polymer HTMs, these layers (ZnO and TiO_x) are in micrometer with dye sensitized. The working principles of these devices are different from each other. In s-DSSC, excited dye inject electrons into TiO_2 nanoparticles whereas in inverted organic solar cell, acceptors materials like (C_{60} or PCBM) are employed to dissociate excition and transfer of electrons. Organic material like spiro-OMeTAD possesses higher PCE in solid-state DSSCs family, where positive charges are transported by hopping processes [56]. But spiro-OMeTAD has low hole mobility and high fabrication cost compared to the conjugated organic polymer materials. P-type conjugated polymer materials are one of the promising materials for hole transportation [57-59].

When TiO_2 layer is sensitized with dye in solid state DSSC, external quantum efficiency (EQE) shows the large contribution of photocurrent generation from the sensitized layer [60-86]. In this architecture, short circuit condition requires the electron injection from the excited dye molecule into conduction band of TiO_2 and transfer of the hole through polymer layer to the back contact electrode. In order to realize this, several requirements have to be fulfilled. The general requirements are [60]

(a) The p-type polymeric material must be highly transparent in the spectral range, where the dye absorbs light.

(b) p-type polymeric material must be available for depositing without dissolving or degrading the dye monolayer on TiO_2 nanocrystallities.

(c) The excited state energy level of dye should be located above the conduction band of TiO_2 and the ground state must be below the upper edge of the valence band of the p-type polymeric material. This is essential for electron transfer from the excited dye molecule to the conduction band of TiO_2 and hole transfer to the valence band of the p-type polymeric material.

Various triarylamine based polymers [61-64], poly(3-alkylthiophene)s [65-77], polypyrrole [78-81], polyaniline [82-86] are studies as HTMs in solid state DSSCs. The polymers cast from solutions must penetrate into the pores between the nanoparticles, and should form a good contact with the absorbed dye. Interestingly, C. S. Karthikeyan et al. [87] demonstrated the self organized interacted molecular between the dye and polymer layers for the efficient transfer of hole from dye to polymer material. Actually, they developed ruthenium complexes carrying different triphenylamine-based donor groups, which combination with a triarylamine material of spiro-MeOTAD. The result indicated that the dye/spiro-MeOTAD interfaces are self-organized by oleophilic interaction resulting in improved photocurrent and efficiency. Similarly, K.J. Jiang et al.[75] reported the dyes with oleophilic thienyl groups, which show power conversion efficiency of up to 2.7%. The authors suggested that the excellent performance is due to the self-organized interface between dye molecules and polymer material

4.3 Laminated solid-state dye sensitized solar cell

In the above section, it was noticed that lamination as a method of OPV devices has several advantages over OPV fabricated from conventional metal evaporation method. Direct metal deposition on the surface of polymeric layer creates high parasitic resistance that reduces the device performance [42-47]. Therefore, it is important to fabricate solid state DSSC from hot plate lamination technique. To our knowledge,

there isn't any report on the fabrication of solid state DSSCs from the hot plate lamination process. Furthermore, we incorporate functionalized MWCNTs (f-MWCNTs) in P3HT solution to improve hole mobility of the device. P3HT was spin coated on the surface of Ru-sensitized titanium dioxide (TiO_2) nanoparticles. Glass/FTO/TiO_2 (Ru dye sensitized) /P3HT//PEDOT:PSS(d-sorbitol)/ITO/PET photovoltaic cells were fabricated. The open circuit voltage (V_{oc}) improved with Au deposited electrode. A small amount of d-sorbitol was added to PEDOT:PSS to improve adhesive properties [41].

4.3.1 Experiment details

FTO substrates were cleaned with acetone, methanol followed by drying in nitrogen gas, it is then ozone treated for 10 mins to remove remaining organic materials from the substrates. A compact layer of TiO_x paste (PASOL HPW-18NR) was spin coated on the cleaned FTO substrate at 2200 rpm for 40 secs. This compact layer removes the possibility of short in the device. In this FTO- TiO_x compact layer, nanoporous TiO_2 slurry was spin coated to make TiO_2 layer of about 2μm thickness. TiO_2 slurry is prepared in the following way. At first, 4 mg of P25 TiO_2 nanoparticles was mixed with 0.4ml acetylacetone (2, 4-Pentanedione) and grind for a few minutes till it changes to light golden color. In the second step, de-ionized water (0.5ml) was poured on it and grind for 5 minutes. At every 5 minutes, the same amount of de-ionized (0.5ml) was added and grinded. This process was repeated for 7 times then 2ml of TritonX (30vol%) was mixed on the solution. Finally, fine PEG (0.4mg) was added to the TiO_2 slurry and grind for a few minutes (10 minutes). The prepared TiO_2 paste was spin coated on the surface of FTO-TIOx layer at 500 rpm for 40 sec.

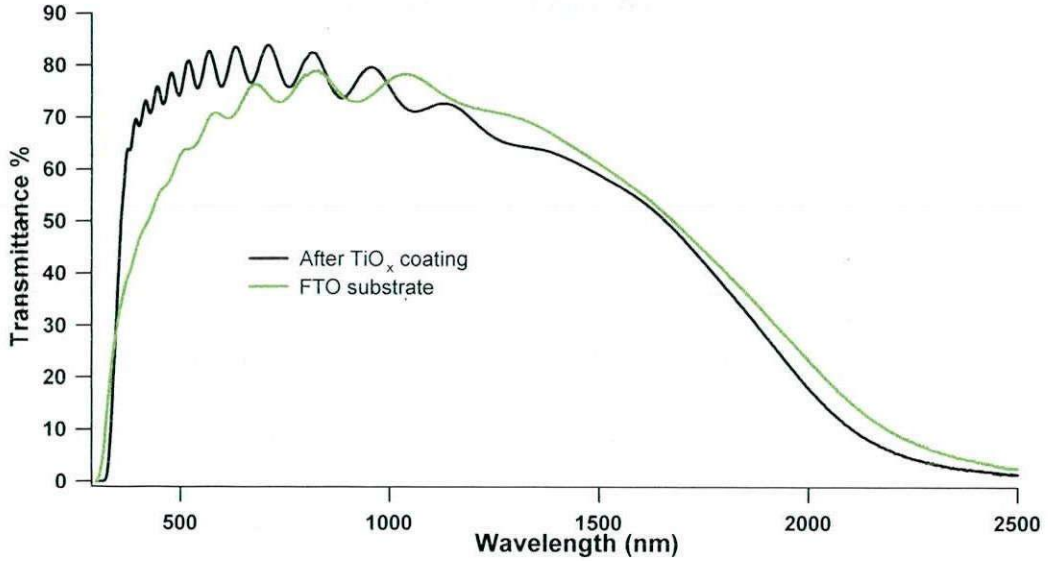

Figure 1. Optical transmission spectra of FTO (red line) and TiO_x coated FTO substrate (black line). Commercially available TiO_x solution (PASOL HPW-18NR) was spin coated.

4.3.2 Result and discussion

Figure 1 shows the improvement in transparency of FTO substrates from 400 nm to 750 nm wavelength after spin coating of TiO_x. The reason for this transmission improvement is unknown at present condition because of the lack of chemical composition of the commercial product (PASOL HPW-18NR).

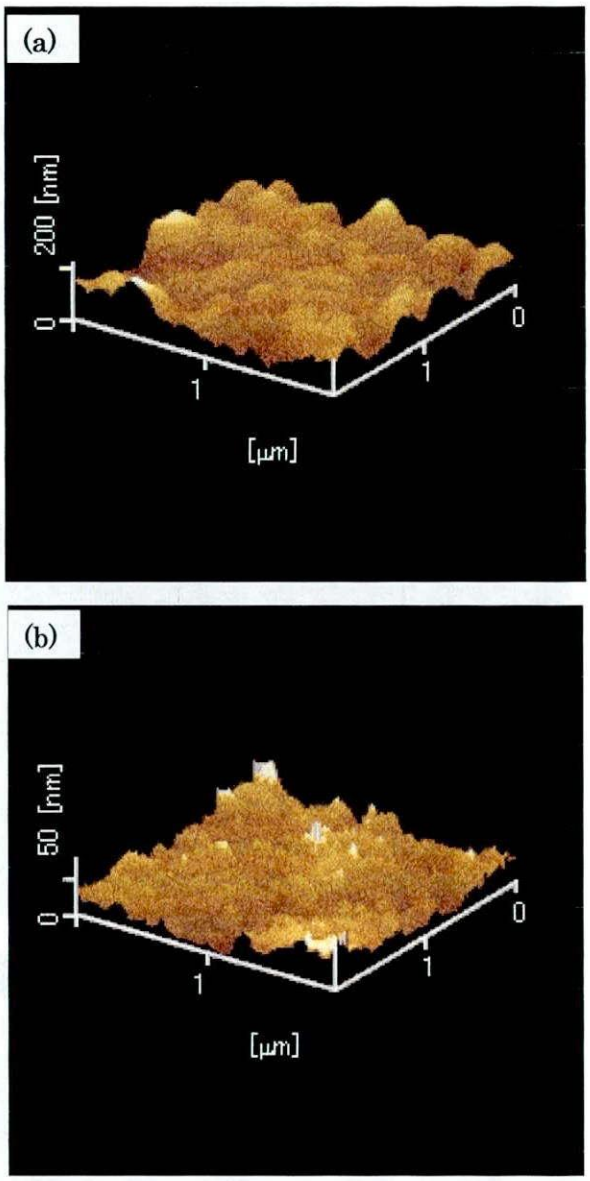

Figure 2. AFM images of FTO before (a) and after (b) TiO_x coating.

Figure 2(a) and (b) show the AFM images of FTO glass substrate before and after spin coating of TiO_x solution, respectively. It depicts that the RMS roughness of FTO substrates reduced from 3.060E+01nm to 8.317 nm and the peak-to-valley (P-V) distance was also reduced from 2.233E+02nm to 7.776E+01 nm. This measurement indicates that the roughness and P-V distance improves after TiO_x coating.

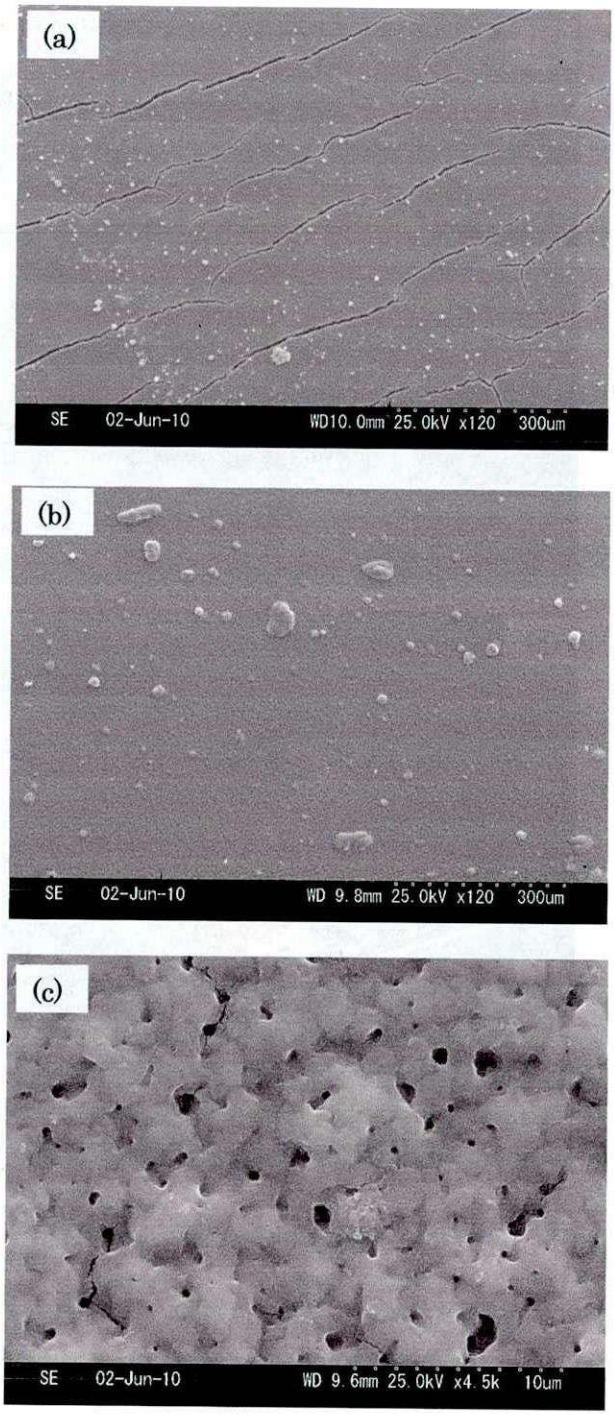

Figure 3: SEM images show (a) cracks on TiO_2 film (b) crack free TiO_2 film after mixing commercial TiO_x paste (c) closer view of TiO_2 film showing microscopic holes

Figure 3 (a) shows the SEM image of the TiO_2 film (not TiO_x) on FTO substrate. After sintering, cracks were observed in the film. With liquid electrolyte, DSSC works well even though the conducting FTO substrate is in direct contact with the electrolyte at the FTO/electrolyte interface. But for solid state DSSC, this becomes the problem. We thought to improve the paste to make crack free titanium layer after sintering. For this, the same amount of commercial available titanium paste (Pasol-HPW-18NR) was mixed with our`s prepared paste with 1:1 ratio. Thin film produced from the mixed TiO_2 paste lacks cracks after sintering as shown in fig 3 (b). The magnificent image of this film in fig 3 (c) shows some microscopic holes like structure on the TiO_2 surface.

TiO_2 coated substrates were sintered at 450°C for 30 min and sensitized with Ru-dye (N719) for 18 hours in ethanol solution. P3HT (17mg/ml) solution in 1, 2-dichlorobenzene was spin coated on the surface of dye-sensitized TiO_2 layer at 2000 rpm for 40 sec. In another set of experiments, f-MWCNTs-P3HT solution was also spin-coated in the similar manner without changing any parameters. This completes the fabrication of one (bottom electrode) part of the laminated solid state DSSC. Another part (top electrode) was prepared in flexible ITO plastic substrate (or Au deposited ITO substrate or Pt deposited substrate) by spin coating PEDOT: PSS (with 10 wt% of D-sorbitol) at 2000 rpm for 40 sec. Finally, the two parts of the device were placed one above another at hot plates and laminated under heat (120°C) and pressure (1.2 Mpa) in air. Before lamination, the edges of the FTO substrates were covered with plastic tape so that the cracked or bare spaces at the edges don't touch the upper electrode.

Figure 4 (a) shows the device configuration of solid state DSSC fabricated from hot press lamination. The melting point of d-sorbitol is about 90~100°C. After reaching to its melting point, it laminates two electrodes electrically and mechanically. It is solvent free electric glue exhibits a conductivity of 10^2S/cm [41]. Figure 4(b) shows the

photograph of the laminated PET/ITO/PEDOT:PSS(d-sorbitol)//P3HT/N719-TiO_2/FTO/glass substrate (the // represent the laminated interfaces) photovoltaic device. The device fabricated without d-sorbitol does not show adhesive properly.

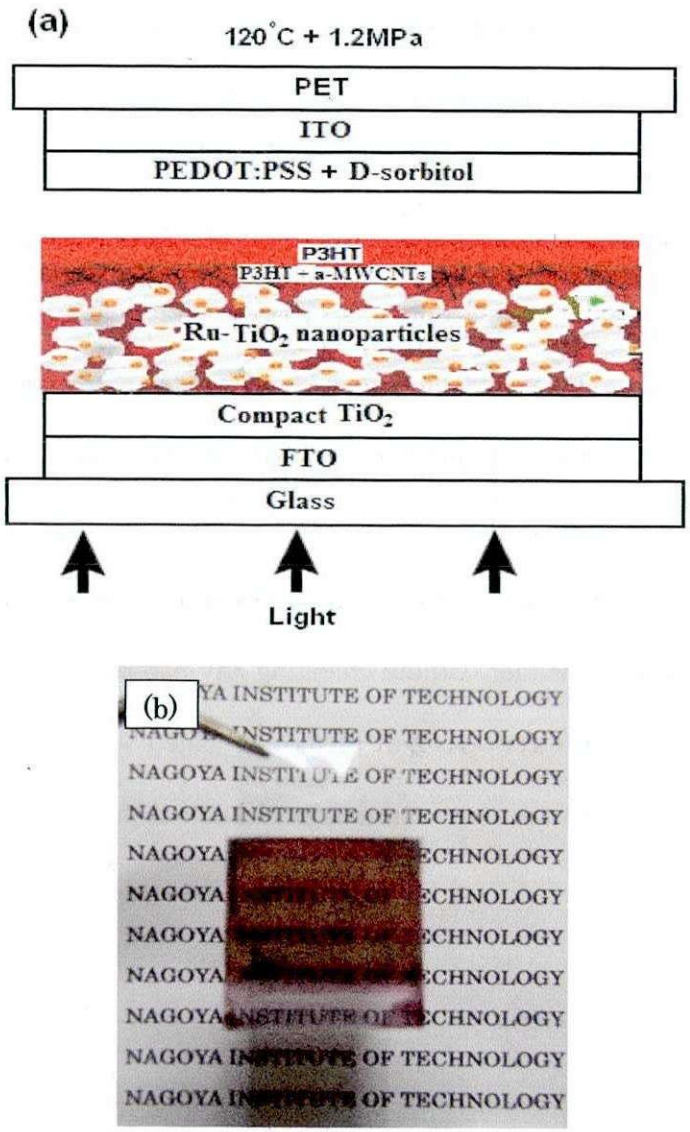

Figure 4.(a) Schematic of PET/ITO/PEDOT:PSS:D-sorbitol//P3HT/Ru-TiO_2/FTO/glass heterojunction solar cell incorporating f-MWCNTs in the polymeric layer, where // represents laminated interface . (b) Photograph of laminated heterojunction solar cell fabricated by hot plate lamination.

Figure 5 shows the J-V characteristics of the photovoltaic devices measured under AM 1.5 simulated solar radiations. The cells were prepared with and without incorporation of f-MWCNT in P3HT solution and illuminated from glass side. The mask of area 1 cm^2 was used during J-V measurement. Under illumination, the device fabricated with P3HT and f-MWCNTs shows J_{sc} and V_{oc} about 1.05mA/cm^2 and 0.04 V, respectively. The fill factor (FF) and white light conversion efficiency (η) is about 0.24 and 0.012%, respectively. A twin reference cell fabricated in the similar manner with only P3HT film shows J_{sc}, V_{oc}, FF and η of 0.12mA/cm^2, 0.06V, 0.25 and 0.0019% respectively. We believe that such improvement using f-MWCNTs might have come from efficient transfer of hole through P3HT and f-MWCNT. The photovoltaic properties that are stated here is just a report on the successful fabrication of solid-state DSSCs from hot plate lamination method. There are a lot of scopes to optimize the device parameters for the improved photovoltaic properties. Sensitizing TiO_2 particles with dye of high molar extinction coefficient, optimization of parameters are some simple ways to improve the device performance.

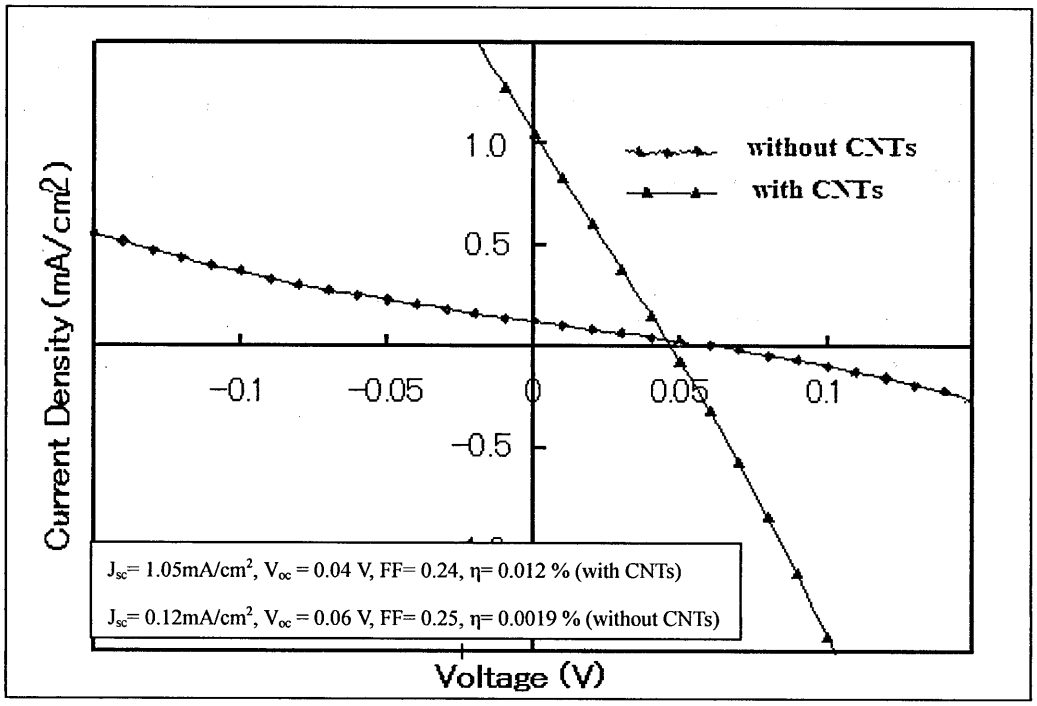

Figure 5. Current voltage (J-V) characteristic of the laminated heterojunction solar cell under AM 1.5 simulated solar radiation with (black line) and without (blue line) f-MWCNTs in polymeric layer.

The initial work shows photovoltaic response of the laminated solid state DSSCs. Improving crystallinity and use of metal electrode is another approach to improve the device performance. One way to improve the crystallinity of the polymer material is by annealing. Therefore, the bottom electrode after P3HT spin coating was annealed at 120°C for 15 min. In doing so, mesocopic order and crystallinity of organic polymer materials increases. From the viewpoint of the relationship between structure and performance, a nanocrystlline structure with high crystallinity is pursued so that a relatively high transportation speed of holes is obtained via interchain transport of charge carriers. After annealing, a very small drop of PEDOT:PSS (with 10% d-sorbitol) solution was drop casted on the surface of P3HT layer. From above, Au deposited ITO PET substrates placed over it. The device is then laminated under heat and pressure.

Under illumination in non-optimized solar cell, J_{sc}, V_{oc}, FF and η are about 0.03 mA/cm^2, 0.1V, 0.27 and 0.001 % respectively. Such improvement in V_{oc} may be due to the crystallinity improvement of P3HT layer or top Au electrode. The light reflection from Au may improve light harvest in the device. Figure 6 shows the J-V characteristics under AM 1.5 simulated solar radiation for laminated solid state DSSC using Au deposited ITO PET substrate in P3HT layer.

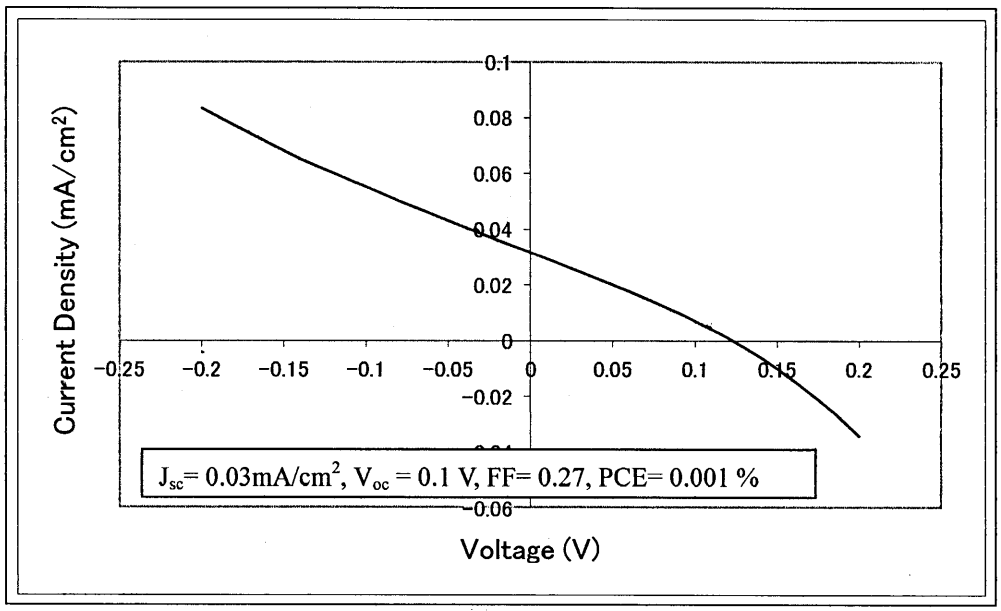

Figure 6. J-V characterization of non-optimized laminated solid state dye sensitized solar cell using metal deposited (Au) electrode on flexible ITO substrates.

Generally, p-type semiconducting polymers that accept holes from the dye cation are important. In FTO/ N719-TiO_2/P3HT//PEDOT:PSS(d-sorbitol)/ITO/PET configuration, we believe that photoexcited dye molecules inject electrons into the conduction band of TiO_2 (E_{cb}~4eV) and hole towards P3HT. The favorable charge transportation is suitable because the excited state energy level of N719 (LUMO~3.7eV) is located above the conduction band of TiO_2 and the ground state (HOMO~5.5eV) level is below the upper

edge of the valance band of the P3HT (E_{vb} ~5.1eV). This is essential for electron transfer from the excited dye molecule to the conduction band of TiO_2 and hole transfer to the valance band of P3HT. P3HT possesses high hole mobility of up to $0.1cm^2V^{-1}s^{-1}$. Similarly, the mobility of MWCNTs is several orders higher in magnitude compared to that of the polymer, which may result in the enhancement of hole transport. In addition, MWCNTs may serve as 'conducting bridges' connecting the polymer chains. The increased work function of f-MWCNTs (5.1eV) efficiently transfer the hole towards PEDOT:PSS. Energetically favorable charge transportation and band diagram is shown in Fig.7.

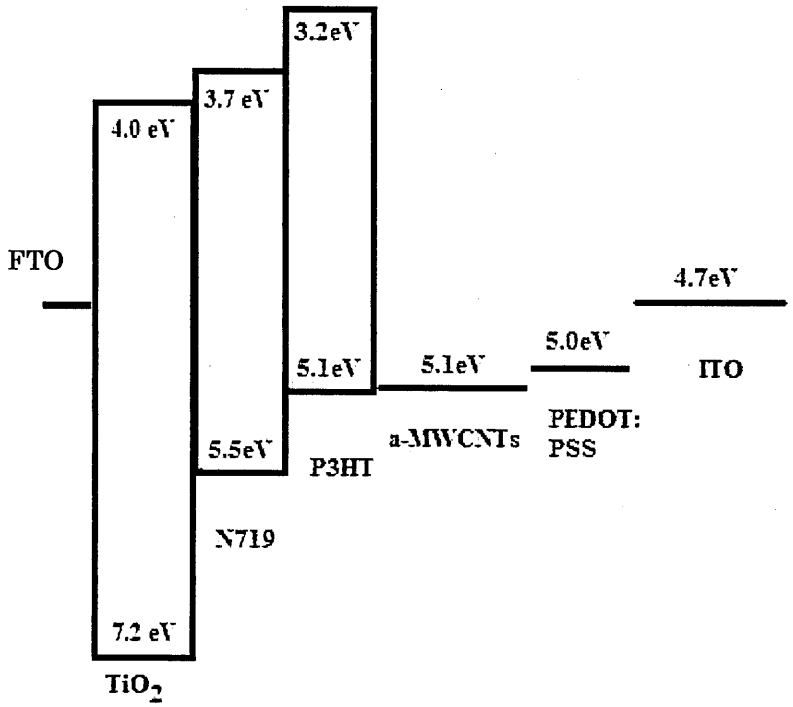

Figure 7. Energy band diagram of the fabricated device showing band alignment.

4.4 Conclusion

Inverted solar cell architecture allows depositing various layers of organic material, metal electrodes onto flexible substrates from solution processing to industrial roll-to-roll manufacture. This device architecture can be further modified by depositing, optimizing and characterizing two parts of the organic layers independently in laminated organic solar cell. The power conversion efficiency of inverted and laminated solar cells is almost same or higher to the power conversion efficiency of devices fabricated from conventional process. The device architecture of these solar cells is similar to the device architecture of solid-state DSSCs that use conjugated polymer as HTMs, which make possible for the fabrication of laminated solid-state DSSCs. The present findings offer novel directions for achieving high-efficiency solid-state DSSC by optimizing and characterizing two different parts of the device independently before bring them to contact. P3HT solutions with and without mixture of MWCNTs were spin coated on the surface of dye sensitized TiO_2 films. Incorporation of MWCNTs in the polymer solution improves the photovoltaic response of the device. Here, it is expected that excited dye molecular inject electron to the conduction band of the TiO_2 layer, whereas MWCNTs and polymer efficiently transfer hole.

References:

[1] J. Y. Kim, S. H. Kim, H.-H. Lee, K. Lee, W. Ma, X. Gong and A. J. Heeger, Adv. Mater. 2006, 18, 572.

[2] A. Yakimov and S. R. Forrest, Appl. Phys. Lett. 2002, 80, 1667.

[3] P. W. M. Blom, V. D. Mihailetchi, L. J. A. Koster and D. E. Markov, Adv. Mater. 2007, 19, 1551-1566.

[4] R. F. Service Science,2011, 332, 293.

[5] G.Dennler, M.C. Scharber, T. Ameri, P. Denk, K. Forberich, C. Waldauf and C.J. Barbec. Adv. Mater. 2008, 20, 579-583.

[6] G. Li, C.-W. Chu, V. Shrotriya, J. Huang and Y. Yang Appl. Phys. Lett. 2006, 88, 253503.

[7] C.-H. Hsieh, Y.-J. Cheng, P.-J Li, C.-H. Chen, M. Dubosc, R.-M. Liang and C.-S. Hsu. J. Am. Chem. Soc.,2010, 132, 4887-4893

[8] M. Glatthaar, M. Niggemann, B. Zimmermann, P. Lewer, M. Riede, A. Hinsch and J. Luther, Thin Solid Films. 2005, 491, 298-300

[9] D.W. Zhao, P. Liu, X.W. Sun, S.T. Tan, L. Ke and A.K.K. Kyaw, Appl. Phys. Lett., 2009, 95, 153304.

[10] F.C. Krebs, Solar Energy Mater. and Solar Cells., 92, 715-726, 2008,

[11] W. Gaynor, J.-Y. Lee and P. Peumans, ACS Nano. 2010, 4, 30-34.

[12] C. Girotto, B.P. Rand, S. Steudel, J. Genoe and P. Heremans, Org. Electron. 2009, 10, 735-740.

[13] S.K. Hau, H.-L. Hip, K. Leong and A. K. –Y. Jen ,Org. Electron., 2009, 10, 719-723

[14] M. S White, D. C. Olson, S. E. Shaheen, N. Kopidakis, and D.S. Ginley, Appl. Phys.Lett., 2006, 87, 143517–143519

[15] S.K. Hau, H.L. Yip, H. Ma and A. K. Y. Jen, Appl. Phys. Lett., 2008, 93, 233304–233306

[16] C. Waldauf, M. Morana, P. Denk, P. Schilinsky, K. Coakley, S.A. Choulis and C.J Brabec, Appl. Phys. Lett., 2006, 89, 233517–233519

[17] R. Steim, S.A. Choulis, P. Schilinsky and C.J. Brabec, Appl. Phys. Lett., 2008, 92, 093303–093306

[18] S.K. Hau, H.L. Yip, O. Acton, N. S. Baek, H. Ma,A.K.Y. Jen, A. K. Y. J. Mater. Chem., 2008, 18, 5113–5119

[19] H.H. Liao, L.-M. Chen, Z. Xu, G. Li and Y. Yang, Appl. Phys. Lett. 2008, 92, 173303-173305.

[20] Y.I. Lee, J. H. Youn, M.S. Ryu, J. Kim, H. T. Moon and J. Jang, Organic Electronics, 2011, 12, 353-357.

[21] D.W. Zhao, S.T. Tan, L. Ke, P. Liu, A.K.K. Kyaw and X.W. Sun, Solar .Energy Maters. & Sol. Cells 2010, 94, 985-991

[22] T.Hori, H. Moritou, N. Fukuoka, J. Sakamoto, A. Fujii, M. Ozaki. Materials 2010, 3, 4915-4921

[23] T. Hori, T. Shibata, V. Kittichungchit, H. Moritou, J. Sakai, H. Kubo, A. Fujii, and M. Ozaki, Thin Solid Films 2009, 518, 522-525

[24] A.K.K. Kyaw, X.W. Sun, C.Y. Jiang, G.Q. Lo, D.W. Zhao, D.L Kwong, Appl. Phys. Lett., 2008, 93, 221107–221109.

[25] C. Tao, S.P. Ruan, X.D. Zhang, G.H. Xie, L. Shen, X.Z. Kong, W. Dong, C.X Liu and W.Y. Chen, Appl. Phys. Lett., 2008, 93, 193307–193309.

[26] H.Schmidt, H. Flugge, T. Winkler, T. Bulow, T. Riedl and W. Kowalsky, Appl. Phys. Lett., 2009, 94, 243302–243304

[27] V. Shrotriya, G. Li, Y. Yao, C.W. Chu and Y. Yang, Appl. Phys. Lett. 2006, 88, 073508

[28] N. Espinosa, H. F.Dam, D. M. Tanenbaum, J. W. Andreasen, M. Jorgensen and F. C. Krebs, Materials 2011, 4, 169-182.

[30] C. Tao, S.P. Ruan, G.H. Xie, X. Z. Kong, L. Shen, F.X. Meng, C.X. Liu, X.D.Zhang, W. Dong, and W.Y. Chen, Appl. Phys. Lett., 2009, 94, 043311–043313.

[31] M.Y. Chan, C.S. Lee, S.L. Lai, M.K Fung, F.L. Wong, H.Y. Sun, K.M. Lau and S.T. Lee, J. Appl. Phys., 2006, 100, 094506–094509

[32]. S.K. Hau, H.L. Yip, H. Ma and A.K.Y. Jen, Appl. Phys. Lett., 2008, 93, 233304–233306.

[33]. C. Waldauf, M. Morana, P. Denk, P. Schilinsky, K. Coakley, S.A. Choulis and C.J. Brabec, Appl. Phys. Lett., 2006, 89, 233517–233519.

[34].R. Steim, S.A. Choulis, P. Schilinsky and C.J Brabec, Appl. Phys. Lett., 2008, 92, 093303–093306

[35] C. Y. Li, T.C. Wen and T. F. Guo, J. Mater. Chem., 2008, 18, 4478–4482.

[36] F.C. Krebs, S.A. Gevorgyan and J. Atstrup, J. Mater. Chem. 2009, 19, 5442-5451

[37] S. K.Hau, H.L. Yip and A. K. Y.Jen Polymer Reviews, 50, 474-510, 2010

[38] M. Nakamura, C. Yang, E. Zhou, K. Tajima and K. Hashimoto, Applied Materials and Interfaces 2009, 1, 2703-2706.

[39] Y. Yuan, Y. Bi and J. Huang Appl. Phys. Lett. 2011, 98, 063306.

[40] B.A. Bailey, M. O. Reese, D. C. Olson, S.E. Shaheen, N. Kopidakis ,Organic Electronics 2011, 12 108-112.

[41] J. Ouyang and Y. Yang Adv. Materials, 2006, 18, 2141-2144.

[42] M. Jorgensen, K. Norrman and F.C. Krebs Sol. Energy Mater. & Sol. Cells, 2008, 92, 686–714.

[43] K. Suemori, T. Miyata, M. Yokoyama and M. Hiramoto, Appl. Phys. Lett. 2004, 85 , 6269–6271

[44] K. Suemori, M. Yokoyama and M. Hiramoto, J. Appl. Phys. 2006, 99, 036109-3.

[45] T. H. Lee, J. C. A. Huang, G.. L. Pakhomov, T. F. Guo, T. C. Wen, Y. S. Huang, C. C. Tsou, C.T. Chung, Y. C. Lin and Y. J. Hsu, Adv. Funct. Mater. 2008, 18, 3036–3042

[46] G. Gu, V. Bulovic, P. E. Burrows, S. R. Forrest and N. E Thompson, Appl. Phys. Lett. 1996, 68, 2606-2608.

[47] H.K. Kim, D.G. Kim, K.S. Lee, M.S. Huh, S.H. Jeong, K.I. Kim and T.Y. Seong, Appl.Phys. Lett. 2005, 86, 183503-183505

[48] K. H. Yim, Z. Zheng, Z. Liang, R.H. Friend, W. T. S. Huck and J. S. Kim Adv. Funct. Mater. 2008, 18, 1012-1019.

[49] L.C. Chen, P. Degenaar & D.D. C. Bradley Adv. Mater. 20, 1679_1683 (2008).

[50] J. H. Huang, Z. Y. Ho, T. H. Kuo, D. Kekuda, C. W. Chu and K. C. Ho J. Mater. Chem. 2009, 19, 4077_4080.

[51] D. H. Wang, D. G. Choi, K. J. Lee, S. H. Im, O. O. Park and J. H. Park, Org. Electron. 2010, 11, 1376-1380.

[52] D. H. Wang, D.G. Choi, K. J. Lee, O.O Park, and J. H. Park, Langmuir 2010, 26, 9584-9588 .

[53] Q. J. Sun, K. Park and L.M. Dai, J. Phys. Chem. C 2009, 113, 7892-7897

[54] M. Nakamura, C. Yang, K. Tajima, K. Hashimoto Solar Energy Materials & Solar Cells 2009, 93 1681-1684.

[55] M. Granstrom, K. Petritsch, A. Arias, A. Lux, M. Andersson and R. Friend, Nature , 1998, 395, 257–260.

[56] U.Bach, D. Lupo, P. Cornte, J.E. Moser, F. Weissortel, J. Salbeck, H. Spreitzer, M. Gratzer, Nature 1998, 395, 583-585.

[57] T. J. Sevenije, J.M. Warman and A. Goossens, Chem. Phys. Lett. 1998, 287, 148.

[58] A.C. Arango, S.A. Carter and P. J. Brock, Appl. Phys. Lett. 1999 74, 1698.

[59] K.M. Coakley, Y. Liu, C. Goh, M.D. McGehee, MRS bulletin, 2005, 30, 37.

[60] D. Gebeyehu, C.J. Brabec, N.S. Sariciftci, D. Vangeneugden, R. Kiebooms, D. Banderzande, F. Kienberger, H. Schindler, Synthetic Metals, 125 (2002) 279-287.

[61] L. Schmidt-Mende, M. Gra¨tzel, Thin Solid Films 2006, 500, 296

[62] J. E. Kroeze, N. Hirata, L. Schmidt-Mende, C. Qrizu, S. D. Ogier, K. Carr, M. Gra¨tzel, J. R. Durrant, Adv. Funct. Mater. 2006, 16, 1832.

[63] K. R. Haridas, J. Ostrauskaite, M. Thelakkat, M. Heim, R. Bilke, D. Haarer, Synth. Met. 2001, 121, 1573.

[64] K. Peter, H. Wietasch, B. Peng, M. Thelakkat, Appl. Phys. A 2004, 79, 65.

[65] J. Roncali, Chem. Rev. 1992, 92, 711.

[66] Y.-J. Cheng, S.-H. Yang, C.-S. Hsu, Chem. Rev. 2009, 109, 5868.

[67] D. Gebeyehu, C. J. Brabec, N. S. Sariciftci, D. Vangeneugden, R. Kiebooms, D. Vanderzande, F. Kienberger and H. Schindler, Synth. Met. 2002, 125, 279.

[68] N. Kudo, S. Honda, Y. Shimazaki, H. Ohkita and S. Ito, Appl. Phys.Lett. 2007, 183513.

[69] C. Zafer, C. Karapire, N. S. Sariciftci and S. Icli, Sol. Energy Mater. and Sol. Cells 2005, 88, 11.

[70] M. Wang and X. Wang, Sol. Energy Mater. Sol. Cells 2007, 91, 1782.

[71] K. Takahashi, T. Nakanishi, T. Yamaguchi, J-i. Nakamura and K. Murata, Chem. Lett. 2005, 34, 714.

[72] E. L. Beltran, P. Prene´, C. Boscher, P. Belleville, P. Buvat and C. Sanchez, Adv. Mater. 2006, 18, 2579.

[73] R. Zhu, C. Y. Jiang, B. Liu and S. Ramakrishna, Adv. Mater. 2009, 21,994.

[74] J. Kruger, R. Plass, L. Cevey, M. Piccirelli, M. Gra¨tzel and U. Bach, Appl. Phys. Lett. 2001, 79, 2085.

[75] K. J. Jiang, K. Manseki, Y. H. Yu, N. Masaki, K. Suzuki, Y. L.Song and S. Yanagida, Adv. Funct. Mater. 2009, 19, 2481.

[76] G. K. Mor, S. Kim, M. Paulose, O. K. Varghese, K. Shankar,J. Basham and C. A. Grimes, Nano Lett. 2009, 9, 4250.

[77] J. A. Chang, J. H. Rhee, S. H. Im, Y. H. Lee, H. J. Kim, S. I. Seok, M. K. Nazeeruddin and M. Gra¨tzel, Nano Lett. 2010, 10, 2609

[78] K. Murakoshi, R. Kogure, Y. Wada and S. Yanagida, Chem. Lett.1997, 471.

[79] K. Murakoshi, R. Kogure, Y. Wada and S. Yanagida, Sol. Energy Mater. and Sol. Cells 1998, 55, 113.

[80] T. Kitamura, M. Maitani, M. Matsuda, Y. Wada and S. Yanagida,Chem. Lett. 2001, 1054.

[81] R. Cervini, Y. Cheng and G. Simon, J. Phys. D: Appl. Phys. 2004, 37,13

[82] S. X. Tan, J. Zhai, M. X. Wan, L. Jiang and D. B. Zhu, Synth. Met. 2003, 137, 1511

[83] S. Tan, J. Zhai, B. Xue, M. Wan, Q. Meng, Y. Li, L. Jiang and D. Zhu, Langmuir 2004, 20, 2934.

[84] S. Tan, J. Zhai, Q. Meng, Y. Li, L. Jiang and D. Zhu, J. Phys. Chem. B 2004, 108, 18693.

[85] H. S. Kim and C. C. Wamser, Photochem. Photobiol. Sci. 2006, 5, 955.

[86] S. Ameen, M. S. Akhtar, G. S. Kim, Y. S. Kim, O. B. Yang and H. S.Shin, J. Alloys Compounds 2009, 487, 382.

[87] C. S. Karthikeyan, H. Wietacsch and M. Thelakkat, Adv. Mater. 2007, 19, 1091

[88] M. Durr, A. Yasuda and G. Nelles, Appl. Phys. Lett. 2006, 89, 061110

[89] H. J. Snaith and M. Gratzel, Appl. Phys. Lett. 2006, 89, 262114

[90] N.Kudo, S. Honda, Y. Shimazaki, H. Ohkita and S. Ito, Appl. Phys. Lett. 2007, 90, 183513

CHAPTER 5

SUMMARY AND FUTURE SCOPE

5.1 Summary

This thesis mainly deals with the synthesis of CNTs and its application to solar cell. CNTs were synthesized by ultrasonic spray pyrolysis. It is a very simple and promising method to grow CNTs at low cost. CNTs were purified, functionalized and mixed with organic materials for the fabrication of hybrid solar cell. Incorporation of CNTs in active layer of hybrid solar cell improves the photovoltaic properties of the device.

Chapter 1 described a short note about carbon materials. It is the most abundant element in the universe. Graphite, diamond, fullerene, carbon nanotubes are all the different allotropes of carbon. It was mentioned that arc discharge, laser ablation, chemical vapor deposition (CVD) are the most commonly used methods for synthesis of CNTs. Moreover, short introduction on polymer and dye sensitized solar cell was also included.

Chapter 2 described the synthesis of carbon nanotubes by ultrasonic spray pyrolysis method. The importance of the system was the availability to produce mist. In our work, we used ethanol as carbon source and nitrogen as carrier gas to transfer the mist into the reaction tube. MWCNTs, SWCNTs, CNFs and CNWs were synthesized successfully. Dip coating of catalyst on silicon substrates was found suitable for the growth of SWCNTs. A few amounts of SWCNTs and MWCNTs were synthesized on zeolite supporting materials. The role of metal catalyst for the formation of SWCNTs was analyzed.

Chapter 3 described the use of CNTs to organic solar cell. CNTs incorporated solar cell showed better power conversion efficiency than pristine cell without CNTs. This was because of the special property of charge dissociation and transport capacity of CNTs. It was mentioned that there are a lot of methods to incorporate CNTs for the fabrication organic solar cell.

Chapter 4 described the fabrication of solid-state dye sensitized solar cell from hot plate lamination. Hot plate lamination as a method to device fabricate have many advantages. The problem of direct metal deposition over the active layer of the organic layer was eliminated. Direct deposition of metal over the active layer may damage the surface of polymer layer and creates high parasitice resistance. In this chapter, we applied the lamination technology to fabricate solid-state DSSC. The materials and techniques used to fabricate laminated DSSC with polymeric HTMs were similar to the techiques used to fabricate inverted organic solar cell.

5.2 Future directions:

Our future step is to fabricate multilayer organic-inorganic heterojunction solar cell.

5.2.1 Fabrication process:

Figure 1 shows the schematic diagram of our future multilayer structure solar cell. Here, polymer layer (with and without acceptor molecular) will be introduced in electrode II. A multilayer device (when two active layers are stacked without interfacial layer) shows J_{sc} that is the sum of two cells [1]. In our work we shall like to fabricate multilayer device by stacking two heterojunction layers of electrode I and II with hot plate lamination technique.

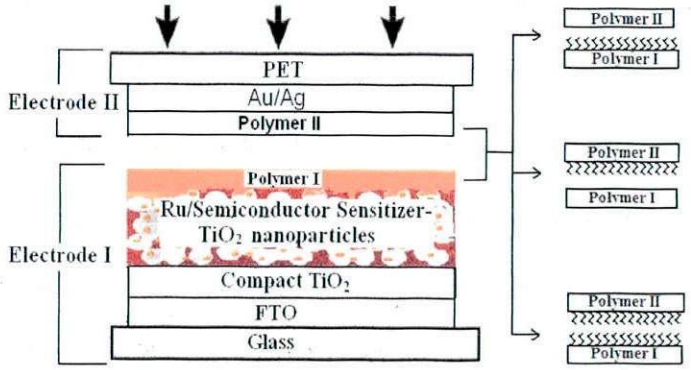

Figure 2. (a) Schematic diagram of the proposed multilayer solar cell. Right hand side shows the surface-segregated monolayer (SSM) in polymer matrix.

5.2.2 Optimization of the device parameters.

At first, the photovoltaic properties of each single layer device will be characterized and optimized. Then the both layers will be stacked to fabricate solar cell. It has been suggested that use of adhesive materials is not necessary when heat and pressure are applied simultaneously [2]. Analysis of absorption spectra, J-V curves and external quantum efficiency (EQE) provide information on the contribution of each layers in multilayer device configuration. To reduce internal resistance at laminated interfaces between polymeric layers, the device will be investigated by modifying the surface properties of polymer so that it generates surface-segregated monolayer (SSM) at top as shown in right hand side of figure 1. The best condition will be characterized. Compounds with low surface energy segregate on the film surface as a monolayer during spin coating of the mixture solution [3]. The contribution of SSM in device performance will be analyzed thoroughly. We believe that the SSM interfacial layer improves adhesive properties of polymer layers or may eliminate or reduce the necessity of heat and pressure during lamination.

5.2.3 Harvesting large portion of visible range of solar light.

To absorb large fraction of sunlight, low and high band gap polymer materials will be used in electrode I and electrode II, respectively. Hot plate lamination technique provides opportunity to fabricate multilayer structures solar cell in simple and easy processes regardless of solvents. Both the layers contribute to the photocurrent generation simultaneously. Optimization of HOMO and LUMO energy level difference is one of the most promising strategies to develop high efficient solar cell. The solar cell will be tested by illuminating the visible light from glass side, therefore light reflection from top metal film further increases the light harvest in the cell.

In short, the above mentioned research plan can be summarized as

- ☐ Fabrication of multilayer organic-inorganic solar cell
- ☐ Optimization of the parameters and understanding the contribution of each layers
- ☐ Introduction of modified donor or acceptor materials to improve adhesive property and remove internal resistance at laminated interfaces
- ☐ Harvesting large fraction of sunlight using sensitizer and low band gap polymer at first electrode and large band gap polymers at second electrode. Light reflection from the metal electrode also improves light harvest.

5.2.4 Expected results and impacts

It is expected that the presented research proposal will provide new ideas and platform to the scientist community to fabricate high efficient organic-inorganic solar cell with improved lifetime. Another important factor of this research is to reduce fabrication cost of solar cell for commercialization. Our target is to achieve more than 7 % efficiency in multilayer organic-inorganic heterojunction solar cell. This study will bring new thoughts to scientific communities. The hot plate lamination technique is also applicable to a wider range of optoelectronic.

References:

1. Q. J. Sun, K. Park and L.M. Dai, J. Phys. Chem. C, 113 (2009) 7892-7897

2. M. Nakamura, C. Yang, K. Tajima, K. Hashimoto Solar Energy Materials & Solar Cells 93(2009) 1681-1684

3. A.Tada, Y. Geng, Q. Wei, K. Hashimoto, K. Tajima, Nature Material 10 (2011) 450-455.

LIST OF PUBLICATIONS

Book Chapter

Chapter 5: Carbon nanotubes towards organic solar cell.

Ishwor Khatri, Tetsuo Soga, Carbon and Oxide Nanostructures (Synthesis, Characteristic and Application) SPRINGER Publication

ISBN: 978-3-642-14672-5

Literatures:

1. Synthesis of single walled carbon nanotubes by ultrasonic spray pyrolysis method.
   Ishwor Khatri, Tetsuo Soga, Takashi Jimbo, Sudip Adhikari, Hare Ram Aryal, Masayoshi Umeno. **Diamond and Related Materials,18 (2009) 319.**

2. Improving photovoltaic properties by incorporating both single walled carbon nanotubes and functionalized multiwalled carbon nanotubes.
   Ishwor Khatri, Sudip Adhikari, Hare Ram Aryal, Tetsuo Soga, Takashi Jimbo, Masayoshi Umeno. **Applied Physics Letters, 94 (2009) 093509.**

3. Synthesis and characterization of carbon nanotubes via ultrasonic spray pyrolysis method on zeolite.
   Ishwor Khatri, Naoki Kishi, Tetsuo Soga, Takashi Jimbo, Sudip Adhikari, Hare Ram Aryal, Masayoshi Umeno.
   Thin Solid Films, 518 (2010) 6756.

4. Synthesis of single walled carbon nanotubes using ultrasonic nebulizer.

   Ishwor Khatri, Tetsuo Soga, Takashi Jimbo.

   IEICE TRANS.ELECTRON. 108 (2008), 41.

5. Simultaneous formation of both single and multi-walled carbon nanotubes by ultrasonic spray pyrolysis

   Ishwor Khatri, Naoki Kishi, Jianhui Zhang, Tetsuo Soga, Takashi Jimbo.

   Japanese Journal of Applied Physics 50 (2011) 020213.

6. Highly oriented carbon nanotubes by chemical vapor deposition.

   Sharif M. Mominuzzaman, Ishwor Khatri, Zhang Jianhui, Tetsuo Soga, Takashi Jimbo. **IEEExplore Electrical and Computer Engineering, 2008. ICECE 2008. International Conference on (2008) 249.**

7. Synthesis of Carbon Nanofibers from Carbon Particles by Ultrasonic Spray Pyrolysis of Ethanol. Jianhui Zhang, Ishwor Khatri, Naoki Kishi, Tetsuo Soga, Takashi Jimbo.

   IEICE TRANS.ELECTRON.,E92-C (2009) 1432.

8. Synthesis of carbon nanofibers using C_{60}, graphite and boron.

   Jianhui Zhang, Ishwor Khatri, Naoki Kishi, Tetsuo Soga, Takashi Jimbo.

   Materials Letters, 64 (2010) 1243.

9. Low substrate temperature synthesis of carbon nanowalls by ultrasonic spray pyrolysis.

   Jianhui Zhang, Ishwor Khatri, Naoki Kishi, Tetsuo Soga, Takashi Jimbo.

   Thin solid Films, 519 (2011) 4162.

10. Catalyst-free synthesis of carbon nanofibers by ultrasonic spray pyrolysis of ethanol.

    Jianfeng Bao, Naoki Kishi, Ishwor Khatri, Tetsuo Soga, Takashi Jimbo.

    Material Letters (accepted manuscript).

11. Fabrication of solid state dye sensitized solar cell from hot plate lamination.

    Ishwor Khatri, Jianfeng Bao, Monshin Ahmad, Naoki Kishi, Tetsuo Soga, Takashi Jimbo (under preparation).

NATIONAL AND INTERNATIONAL CONFERENCES:

1. Title: Synthesis of single walled carbon nanotubes by ultrasonic spray pyrolysis method.

Authors: Ishwor Khatri, Tetsuo Soga, Takashi Jimbo, Sudip Adhikari, Hare Ram Aryal, Masayoshi Umeno.

Organizer: **The 2nd International Conference on New Diamond and Nano Carbons 2008**, Taipei, Taiwan.

2. Title: Synthesis of Single Walled Carbon Nanotubes using Ultrasonic Nebulizer.

Authors: Ishwor Khatri, Sharif M. Mominuzzaman, Tetsuo Soga, Takashi Jimbo.

Organizer: **The Japan Society of Applied Physics (JSAP)**, Chiba, 2008, Japan.

3. Title: Synthesis of carbon nanotubes and thin film fabrication.

Authors: Ishwor Khatri, Tetsuo Soga, Takashi Jimbo, Sudip Adhikari, Hare Ram Aryal, Masayoshi Umeno.

Organizer: **Nano-SciTech 2008**, Selangon, Malaysia.

4. Title: Improvement of photovoltaic properties by incorporating carbon nanotubes.

Authors: Ishwor Khatri, Sudip Adhikari, Hare Ram Aryal, Naoki Kishi, Tetsuo Soga, Takashi Jimbo, Masayoshi Umeno.

Organizer: **The Japan Society of Applied Physics (JSAP)**, Toyama, 2009, Japan.

5. Title: Improving photovoltaic properties by incorporation carbon nanotubes and growth mechanism of nitrogen doped carbon nanotubes on silicon substrate;

Authors: Ishwor Khatri, Naoki Kishi, Tetsuo Soga, Takashi Jimbo

Organizer: **1st Nanomaterial seminar for reducing environment risk, Jenesys Program**, Nagoya Institute of Technology 2009, Japan

6. Title: Formation of single wall carbon nanotubes on fluorine doped tin oxide and its application for dye sensitized solar cell.

Authors: Ishwor Khatri, Naoki Kishi, Tetsuo Soga, Takashi Jimbo

Organizer: **4th International Workshop on Advanced Ceramics, IWAC04, 2010**, Nagoya Institute of Technology, Japan

7. Title: Liquid nitrogen treated fluorine doped tin oxide substrate for dye sensitized solar cell.

Authors: Ishwor Khatri, Naoki Kishi, Tetsuo Soga, Takashi Jimbo.

Organizer: **Nano-SciTech 2011**, Shah Alam, Malaysia

ACKNOWLEDGEMENT

First and foremost I would like to thank my academic supervisor, **Professor Tetsuo Soga** for taking a chance on me when I knew very little about carbon materials and photovoltaic systems at the start of my doctoral studies. I am grateful that he allowed me flexibility in conducting my research and his guidance is greatly appreciated.

My sincere gratitude to **Professor Masayoshi Umeno**, Chubu University for his support and guidance to improve the quality of carbon research. I feel very fortunate to have had Professor Masayoshi Umeno.

I am also grateful to my thesis co-advisors, **Professor Shinji Kawasaki**, Department of Materials Science and Engineering, Nagoya Institute of Technology, Japan and **Associate Professor Yasuhiko Hayashi**, Department of Frontier Materials, Nagoya Institute of Technology, Japan, for their comments to improve this thesis more quality.

These years of study were made much easier and extremely entertaining with the help and support of **Professor Takashi Jimbo**, Research Center for Nano-Device and System, Nagoya Institute of Technology and **Associate Professor Naoki Kishi**, Department of Frontier Materials, Nagoya Institute of Technology, Japan. I thank them for their help and advice with lab equipment and experimentation.

My special thanks and gratitude to **Dr. Sudip Adhikari**, Chubu University, **Dr. Pradeep Khatri**, Chiba University and **Mr. Pradhumna Khatri** for their thorough evaluation, critical comments and valuable suggestions. I learned a lot of things from them.

My special thanks to **Dr. Hari Ram Aryal, Dr. Yasser A.M. Ismail, Dr. Rakesh Afre, Dr. Pradip Ghosh, Dr. Jianhui Zhang, Mr. Jianfeng Bao** and **Mr. Monshin Ahmad** for their valuable help and cooperation in conducting experiments and academic discussion. I also thank to **Mr. Ezaka Kasuke** and other Japanese members of my laboratory for their valuable help, cooperation during experimental works.

I highly acknowledge to **Hirose International Scholarship Foundation** for providing scholarship and **NGK International House** for providing clean room to stay at very low price.

I would like to extend my whole hearted thanks to my parents, brothers and sisters for their love, support and encouragement.

Ishwor Khatri

Nagoya Institute of Technology, Nagoya, Japan

March, 2012